Biophysical Journal
Article

Biophysical Society

Transient Thresholding: A Mechanism Enabling Noncooperative Transcriptional Circuitry to Form a Switch

Katherine H. Aull,[1] Elizabeth J. Tanner,[2] Matthew Thomson,[3] and Leor S. Weinberger[2,4,*]
[1]Bioinformatics Graduate Group, University of California, San Francisco, San Francisco, California; [2]Gladstone Institutes (Virology and Immunology), San Francisco, California; [3]Division of Biology and Biological Engineering, Caltech, Pasadena, California; and [4]Department of Biochemistry and Biophysics, University of California, San Francisco, San Francisco, California

ABSTRACT Threshold generation in fate-selection circuits is often achieved through deterministic bistability, which requires cooperativity (i.e., nonlinear activation) and associated hysteresis. However, the Tat positive-feedback loop that controls HIV's fate decision between replication and proviral latency lacks self-cooperativity and deterministic bistability. Absent cooperativity, it is unclear how HIV can temporarily remain in an off-state long enough for the kinetically slower epigenetic silencing mechanisms to act—expression fluctuations should rapidly trigger active positive feedback and replication, precluding establishment of latency. Here, using flow cytometry and single-cell imaging, we find that the Tat circuit exhibits a transient activation threshold. This threshold largely disappears after ~40 h—accounting for the lack of deterministic bistability—and promoter activation shortens the lifetime of this transient threshold. Continuous differential equation models do not recapitulate this phenomenon. However, chemical reaction (master equation) models where the transcriptional transactivator and promoter toggle between inactive and active states can recapitulate the phenomenon because they intrinsically create a single-molecule threshold transiently requiring excess molecules in the inactive state to achieve at least one molecule (rather than a continuous fractional value) in the active state. Given the widespread nature of promoter toggling and transcription factor modifications, transient thresholds may be a general feature of inducible promoters.

INTRODUCTION

Thresholds allow biological systems to either respond to or disregard a signaling input, based on the input's strength or level. Such thresholds are critical for cellular decision-making and are often a key design feature of gene-regulatory circuits, enabling the regulatory circuit to be robust to spurious signals or noise (1–3). Historically, the mechanism for threshold generation was thought to be either the presence of deterministic multistability (4–6) or zero-order ultrasensitivity (7,8), both of which require specific regulatory architectures (high-order self-cooperativity with hysteresis and zero-order oppositional reactions, respectively). For example, if a putative activator molecule requires homodimerization (i.e., self-cooperativity) to become functional, this automatically generates a molecular threshold—determined by the dimerization disassociation constant—and can lead to deterministic bistability; below the dimerization threshold, there is no functional activator, whereas above the threshold, activation ensues.

Formally, deterministic multistability requires nonlinearity in the governing differential equations, which can be achieved by self-cooperative positive feedback:

$$\frac{dX}{dt} = \frac{a \times X^H}{k + X^H} - r \times X,$$

where X is the activator, a is the feedback strength, k is a Michaelis constant, r is the decay rate, and H is the Hill coefficient (Fig. 1 *A*, *left*). When the positive feedback is self-cooperative (i.e., $H > 1$), the circuit can exhibits deterministic multistability; in particular, if $H = 2$, the system can be bistable with two stable states (ON and OFF) separated by an unstable state, the separatrix. Bistable circuits exhibit a response threshold (specifically, at the unstable separatrix) and are characterized by hysteresis, a type of memory in which the circuit produces different dose-response curves, depending on whether signal increases or decreases (6). In contrast, positive-feedback circuits lacking self-cooperativity ($H = 1$) are monostable, having no separatrix (or threshold), no hysteresis, and only a single stable state; if this circuit can be turned ON, then the only stable

Submitted December 9, 2016, and accepted for publication May 1, 2017.
*Correspondence: leor.weinberger@gladstone.ucsf.edu
Editor: Nathalie Balaban.
http://dx.doi.org/10.1016/j.bpj.2017.05.002

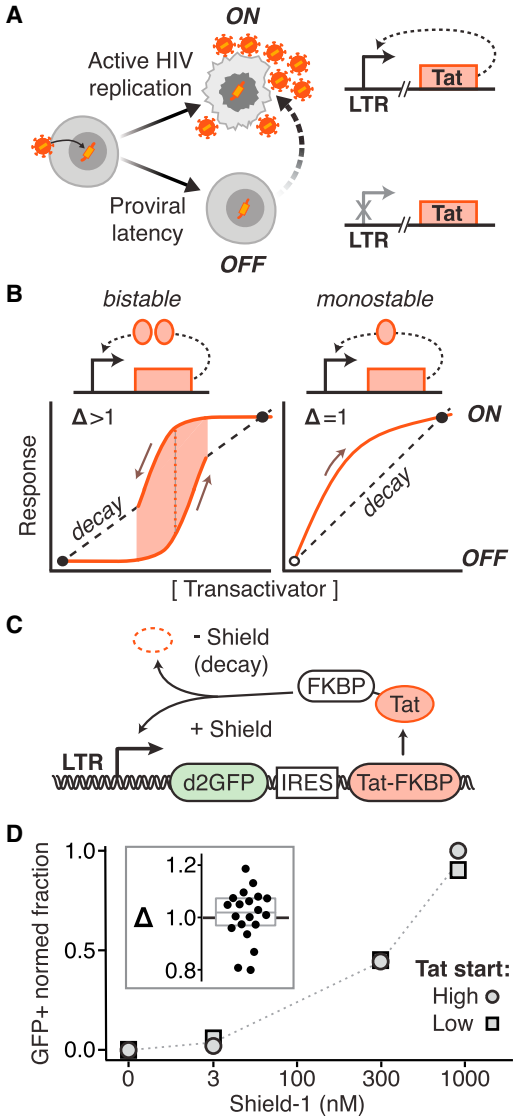

FIGURE 1 The HIV LTR-Tat positive-feedback circuit lacks hysteresis and bistability. (*A*) Given here is the schematic of the HIV fate decision between active replication (ON) and latent (OFF) states. This fate decision is controlled by the HIV Tat-LTR positive-feedback circuit. Transactivation of LTR, the sole promoter of HIV, by its gene product Tat drives further Tat production and HIV replication. (*B*) Given here is bistability versus monostability in positive-feedback transcriptional circuits. Formally, deterministic multistability requires nonlinearity in the governing differential equations (6); for example, if the activator requires cooperative self-association to bind its promoter, its expression is described by a nonlinear Hill equation (Hill coefficient $H > 1$) (20). Such circuits exhibit bistability, having two attractor states (ON and OFF) separated by a response threshold—at low activator levels, the decay rate (*dashed line*) dominates over synthesis (*solid line*), and at high levels, the opposite is true—and hysteresis, a type of memory in which the response is history dependent, following different paths from ON-to-OFF versus OFF-to-ON (the difference between paths is $\Delta > 1$). In contrast, circuits lacking self-cooperativity ($H = 1$) are monostable, having neither a threshold nor hysteresis ($\Delta = 1$)—if a monostable circuit can be turned ON, its only stable state is the ON-state (assuming the biochemical rate constants are not changing), with the OFF-state being necessarily unstable (6). (*C*) Given here is a schematic of the minimal HIV Ld2GITF positive-feedback circuit used to test for hysteresis (LTR driving a 2-h half-life GFP reporter and an internal ribosome entry site expressing Tat fused to FKBP, a degradation tag inactivated by the small molecule Shield-1). (*D*) Given here is a hysteresis test by flow cytometry analysis of Ld2GITF. Isoclonal Jurkat Ld2GITF cells were either pretreated with 1 μM Shield-1 for four days to activate cells to start in an ON state (*oval data points*) or not pretreated to start in an OFF state (*square data points*). All cells were washed and then incubated in the specified Shield-1 alongside for an additional four days, and the percentage of GFP+ cells was measured. (*Inset*) Δ (the ratio of pretreated to not-pretreated GFP+ cells) calculated for five isoclonal populations of Ld2GITF ($\langle\Delta\rangle \approx 1$).

state is the ON state (assuming the biochemical rate constants are not changing), with the OFF state being necessarily unstable (Fig. 1 *A*, *right*).

Gene-regulatory circuits typically achieve $H > 1$ and bistability via cooperative binding of a transcription factor to its promoter (9,10). Notable examples of bistable gene-regulatory circuits include the toggle switch (11), phage-λ lysis-lyogeny (12,13), the lac operon (14), and competence in *Bacillus subtilis* (15,16), all of which have thresholds established by high-cooperativity feedback loops. Other mechanisms for generating a threshold include zero-order ultrasensitivity (7,8) and buffered threshold-linear responses (17,18); however, when applied to transcription-factor induction of a promoter, these models (19) either fail to generate a threshold response (see Supporting Material) or rely on an excess of substrate (i.e., the promoter itself) (20), respectively.

In stark contrast to these canonical examples, the circuit that controls HIV's fate decision between active replication and proviral latency (Fig. 1 *B*) appears to lack the classic mechanisms associated with deterministic bistability or ultrasensitivity (21). Latent HIV is the chief barrier to a cure (22) and the decision between active replication and latency in HIV is governed primarily by the virus's positive-feedback circuit in which HIV Tat protein transactivates expression of the HIV long terminal repeat (LTR) promoter, the only promoter in the virus (Fig. 1 *B*). During latency, the LTR is largely quiescent but establishment of latency is not correlated with viral integration site (23–25) or progressive cellular silencing (26). Specifically, epigenetic silencing occurs on the order of weeks (27), whereas ~50% of infections result in immediate establishment of latency in vitro (28,29), and latency is established within 72 h in vivo (30). Overall, latency establishment occurs too quickly to be accounted for by epigenetic silencing, which acts on timescales of weeks in T cells (27). Instead, the data appear more parsimonious with the Tat-LTR positive-feedback circuit being necessary and sufficient for establishment of latency (26), whereas long-term stability of latency is likely mediated by epigenetic silencing (31).

Tat acts as a monomeric transactivator, binding to a single site on a nascent RNA hairpin formed by stalled RNA polymerase II at the LTR promoter. Because Tat binds noncooperatively, classical deterministic models predict that the circuit should have no activation threshold and thus the

latent state would be unstable (32). Thus, it is unclear how, without bistability, HIV generates a molecular threshold in Tat so that it can even temporarily remain in an off-state and provide an opportunity for the kinetically slower epigenetic silencing mechanism to act. Given the noisy expression of the HIV LTR promoter (33,34), Tat positive feedback should trigger active replication within these first few days. This would preclude establishment of proviral latency, as active replication destroys the cell within hours (35) and silencing of an actively replicating cell cannot overcome active HIV gene expression (26). In general, it remains unclear how the Tat positive-feedback circuit that lacks deterministic bistability (and ultrasensitivity) can generate a threshold to establish a stable off-state.

Here, we examine the HIV Tat-LTR circuit to determine how a threshold can be generated without self-cooperativity. Using a combination of single-cell experimental analyses, both flow cytometry and time-lapse fluorescence microscopy, we find that the LTR circuit exhibits a transient threshold for activation by Tat. The threshold gradually disappears, and at ~40 h, there appears to be no effective threshold such that the LTR-Tat circuit exhibits no hysteresis or deterministic bistability. Cellular activation (e.g., NF-κB signaling), which modulates the kinetics of promoter toggling, shortens the transient lifetime of the threshold. Stochastic models where the transcriptional transactivator and promoter toggle between inactive and active states appear sufficient to recapitulate the transient-threshold phenomenon.

MATERIALS AND METHODS

Cell lines and reagents

The minimal Ld2GITF feedback circuit and the doxycycline-inducible Tat-Dendra cell line have been described in Razooky et al. (26). Here, the lentiviral LTR mCherry reporter from Razooky et al. (26) was modified to contain an N-terminal PEST tag, giving LTR mCherry-deg, with mCherry protein half-life 10.7 h (data not shown; plasmid maps and cloning details available on request). LTR mCherry-deg was packaged in 293T cells and used to infect Jurkat Tat-Dendra cells at low MOI (mCherry positive cells <5%). These cells were induced at high doxycycline (Dox, 500 ng/mL) for 2 days, and FACS sorted with a FACSAria II (BD Biosciences, San Jose, CA) to isolate dual-positive single cells that were grown into isoclonal populations. Isoclones were screened to confirm robust dual-positive response to Dox with negligible expression at baseline. Unless otherwise stated, all chemical reagents were sourced from Sigma-Aldrich (St. Louis, MO). When specified, the HIV reactivating agents tumor necrosis factor alpha (TNFα, 10 ng/mL) or trichostatin A (TSA, 400 nM) were supplied at the time of Dox addition.

Flow cytometry data collection and analysis

To generate dose-response plots, each isoclone and condition was tested at eight Dox levels: seven twofold dilutions, from 250 to 3.9 ng/mL, plus a zero-Dox control. Data were collected on a MACSQuant high-throughput flow cytometer (Miltenyi Biotec, Bergisch Gladbach, Germany), gated for live single cells in FlowJo (Tree Star, Ashland, OR). The mCherry positive cutoff was chosen to exclude noninduced cells. All eight Dox dilutions were pooled and cells were grouped by Tat-Dendra signal to estimate the conditional probability of LTR response for the specific Tat level. A schematic of this workflow, with sample data, is presented in Fig. 2, *B–D* (all Tat-Dendra values were background-subtracted, using the mean of zero-Dox control as background; clusters with nonpositive Tat-Dendra values not considered in the analysis). The dose-response and dose-mean expression curves obtained by this method were fit to a standard Hill function: $P_{ON} = P_{MAX} \times (Tat^H/(K_{50}^H + Tat^H))$. Nonlinear least-squares fitting was performed in the programming language R, using the nlsLM function from the minpack.lm package (Comprehensive R Archive Network/CRAN; https://cran.r-project.org/).

Immobilization of cells for time-lapse imaging

A quantity of 5–10 $\times$ 10^6 actively dividing (healthy) Jurkat cells was washed twice in regular phosphate-buffered saline (PBS), then again in mildly alkalized PBS (pH 8.0). Immediately before use, a single aliquot of biotinylation reagent (1 mg EZ-Link Sulfo-NHS-LC-Biotin; Thermo Fisher Scientific, Waltham, MA) was resuspended in 800 μL PBS (pH 8.0). Of this, 500 μL was used to resuspend the cells after the final wash, whereas the rest were added to a collagen-coated coverslip plate (No. 1.5, 35 mm; MatTek, Ashland, MA). Both cells and coverslip were kept at room temperature. After 30 min, the coverslip was thoroughly rinsed with PBS + 50 mM glycine, then coated with 80 μL streptavidin (1 mg/mL; New England Biolabs, Ipswich, MA). The cells were washed twice in glycine solution, then again in standard culture medium. During the final wash step (~15 min later), the coverslip was rinsed with PBS to remove unbound streptavidin. The biotinylated cells were resuspended in ~300 μL culture medium, transferred to the coverslip, then placed in the incubator for 30 min to settle by gravity. Unbound cells were then carefully rinsed away, and the plate was refilled with 2.5 mL of culture medium containing 250 ng/mL Dox. The finished plate was placed on the microscope for thermal equilibration (~1 h) and subsequent imaging.

Microscope setup and imaging conditions

All imaging was performed on an Axiovert inverted fluorescence microscope (Carl Zeiss, Oberkochen, Germany), equipped with a Yokogawa spinning disk, a CoolSNAP HQ2 14-bit camera (PhotoMetrics, Tucson, AZ), and laser lines for 488- and 561-nm excitation. To facilitate time-lapse imaging, the microscope has a programmable stage with definite focus, and also a stage enclosure that maintains samples at 37°C and 5% CO_2 with humidity. Images were captured every 10 min, sampling a 5 $\times$ 5 *X-Y* grid, one *Z* position each. Exposures were 800 ms at 20% power with the 561-nm laser, then 400 ms at 10% power with the 488-nm laser, then 600 ms for bright field. The objective used was a 40$\times$ oil, 1.3 NA, with 2 $\times$ 2 camera binning applied. For all "induced Tat" movies, imaging was started no more than 2.5 h after Dox addition, and was continued until 20 h. For protein half-life measurements, imaging was started 10 min after addition of 10 μg/mL cycloheximide and continued for 50 10-min intervals. Bleaching half-life was measured with the same image settings, but taken at one location in 5-s intervals to minimize changes in total protein level. For HSV-GFP imaging, to maximize the visibility of these very small particles, the 488-nm exposure time was increased to 40 s and binning was turned off. For each location in a 7 $\times$ 7 X-Y grid, nine *Z* positions were sampled at 0.2 μm intervals; the most in-focus image was chosen for analysis.

Image segmentation analysis to generate single-cell trajectories

The center of each cell was manually marked, using the final bright field image and a custom script (MATLAB; The MathWorks, Natick, MA). For each cell location, a 23-pixel-diameter circle was marked around it,

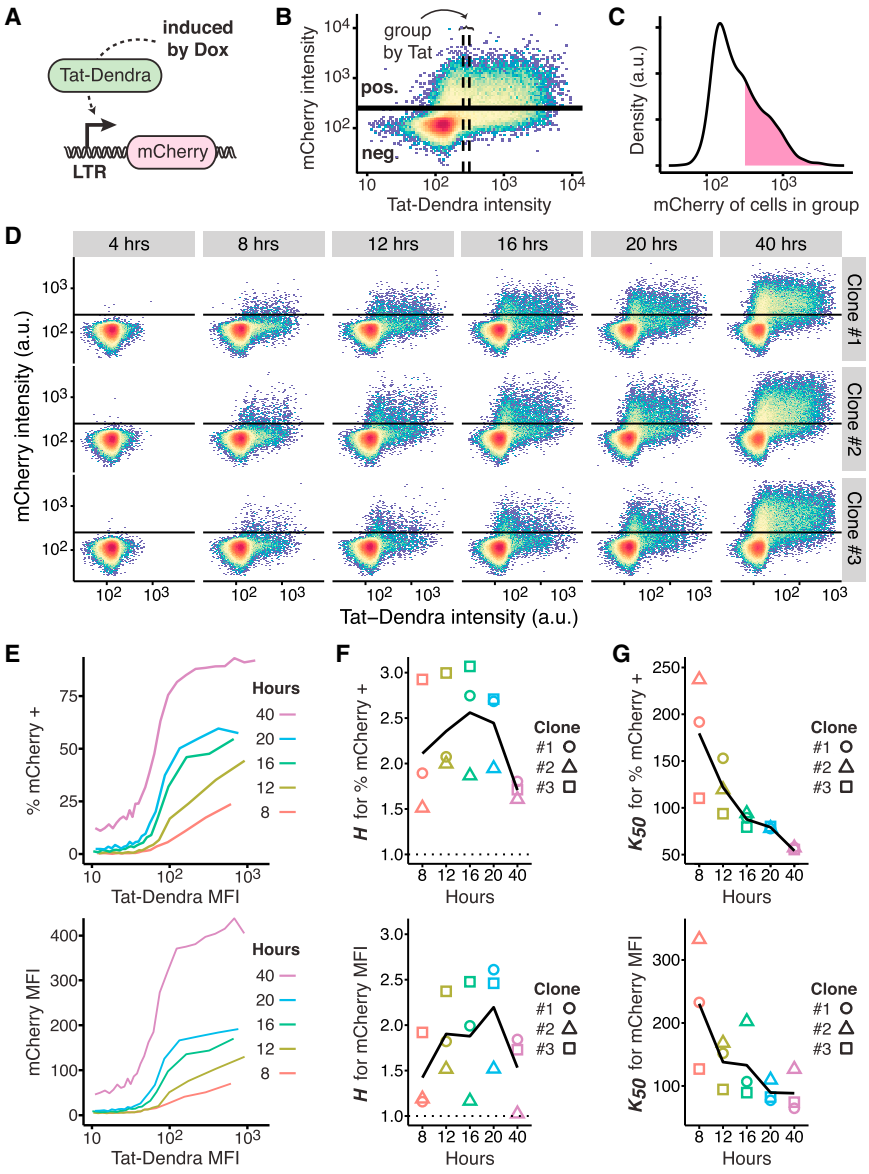

FIGURE 2 The LTR promoter exhibits a transient threshold in its response to Tat. (*A*) Given here is a schematic of constructs used to directly quantify LTR-Tat dose-response function. A doxycycline-inducible promoter (Tet-ON system) drives expression of a Tat-Dendra2 fusion protein, which activates the LTR promoter to drive expression of destabilized mCherry reporter. (*B*) Given here is a scheme for estimating conditional probability of LTR activity for a given Tat level, with a representative two-color flow cytometry dot plot of an isoclonal Jurkat cell line stably expressing constructs in (*A*) after 20 h of Dox induction (plot shown is Clone #2). To estimate the conditional probability of LTR expression for a given Tat level, data were combined from eight Dox dilutions (0–250 nM). The dense spot in the lower-left corner corresponds to noninduced cells (i.e., autofluorescence background), which the mCherrypositive cutoff gate excludes (as indicated by the *black horizontal line*). Cells with similar Tat-Dendra values were grouped, as indicated by the vertical dashed lines, and the percentage of cells above the mCherrypositive cutoff and mean mCherry fluorescence was recorded for each group. For visual clarity, this panel depicts a group of 2500 cells, whereas the analysis uses a tighter group of 1000 cells. (*C*) Given here is a histogram of mCherry intensity for cells in the marked group. Density above the mCherrypositive cutoff is shaded. Despite the narrow band of Tat-Dendra intensities, the LTR response is variable. (*D*) Given here is the full-flow cytometry time-course for three isoclones of Jurkat encoding both Tet-Tat-Dendra and LTR-mCherry-deg induced with eight Dox dilutions, and measured by flow cytometry over time. Horizontal lines indicate the mCherry positive cutoff. At early times, a pronounced shoulder is visible in Tat expression where a substantial percentage of cells express Tat-Dendra but these cells do not express mCherry from the LTR. (*E*) Given here are calculated dose-response curves for % of mCherry+ cells (*top*) and mCherry MFI (*bottom*) from data in (*D*). Clone #1 is shown; the other isoclones, and Hill fits, are presented in Fig. S1. (*F*) Given here are calculated Hill coefficients (H) from dose-response curves over time. The expected noncooperative response ($H = 1$) is indicated by a dashed line; all data points are above the expected $H = 1$ line. Maximum H-values occur at intermediate time points for both % of mCherry cells and MFI. (*G*) Given here is calculated half-maximal response (K_{50}) from fits of the dose-response curves over time. K_{50} declines over time, indicating that the threshold becomes progressively weaker.

and the mean fluorescence intensity within that circle was recorded at each time point to generate single-cell trajectories. Each trajectory was then subjected to automated quality control (QC): cells in which any two consecutive readings differed by >15% in either channel were excluded; upon review of the source images, these events were typically due to cell division, or another cell drifting into view. Cells that began the experiment ON were also excluded (LTR >2% over background at 2.5 h post-Dox addition; this was rare, 2–5 cells per condition). Illustrations of the raw image data and QC process are available in Fig. S2. For these movies, between 2001 and 2193 cell trajectories passed QC. The trajectories were normalized to set their lowest values to zero, then fit to a smoothing spline in base R (df = 10, n = 105) to further reduce noise. Tat-Dendra trajectories were also corrected for photobleaching. This was not necessary for mCherry, which did not bleach under the imaging conditions used (data not shown). The photobleaching correction process is described in Fig. S3.

Quantitation of Tat-Dendra molecular number by GFP molecular rulers

For quantitation using the HSV-GFP molecular ruler (36,37), the images of viral particles were processed using a custom script (MATLAB). Each image was background subtracted, using the median of all 49 images as background, then thresholded to include the bright particles and the first Airy disk surrounding them. The MATLAB function bwconncomp was used to identify potential features within the images. To set the correct size, TetraSpeck beads (Thermo Fisher Scientific, Waltham, MA) were analyzed by the same method; the 0.2-μm beads were 15–18 pixels (data not shown). Because the HSV-1 capsid is 125 nm (38), features between 10 and 14 pixels were selected. For each feature, the total intensity above background was recorded. The mean value was 1424 units (95% cumulative index (CI), 1412–1435; n = 5004.). Given that the HSV-GFP images had

100× the exposure time, and 4× as many pixels, relative to the Tat-Dendra images, each intensity unit of HSV-GFP represents 25× less signal. EGFP is also brighter than Dendra2 by 1.47× (39) such that there are [1424:25] intensity equivalents per [900 × 1.47] molecular equivalents, which reduces to 1 intensity unit per 23.2 Tat-Dendra (Fig. S4). From the single-cell imaging data, the threshold level of Tat proteins required to minimally activate the LTR (i.e., >2% mCherrypositive cells) gives an intensity signal of 5.0 units per pixel, or 1900 units per cell (each cell is 377 pixels). The conversion factor calculated from molecular ruler thus estimates the minimal activation threshold at 4.4×10^4 Tat molecules per cell (Fig. 3 *C*).

Computational modeling

Deterministic and stochastic computational modeling (Supporting Material and Fig. 5, respectively) was carried out in Mathematica (Wolfram Research; https://www.wolfram.com/mathematica/). Deterministic ordinary differential equation (ODE) models of Tat transactivation of the LTR were based on generalized mathematical models of ultrasensitive responses (19) and previous experimentally validated LTR-Tat circuit models (32) that incorporate reversible acetylation-deacetylation of Tat protein (i.e., so-called "futile cycles"). For stochastic models of chemical master equations, the two-state model of the LTR promoter (33,40–42) was simulated by Gillespie's method (43) using the Mathematica xSSA package (http://www.xlr8r.info/SSA/). The outputs from simulations are presented in arbitrary numbers. Initial conditions for all species were set to 0 (except $LTR_{OFF} = 1$) and simulations were run to time = 200 (arbitrary time units). 200 simulations were run per model and parameter set, and mean Tat and mCherry values for all runs were calculated at specified time points.

RESULTS

The HIV LTR-Tat circuit lacks hysteresis and bistability

Previous studies demonstrated that the HIV Tat-LTR positive-feedback loop exhibits a purely linear expression rate at early times (i.e., scales linearly with Tat and lacks cooperativity) (32), as expected for noncooperative positive feedback (Fig. 1 *A*). To confirm that the LTR-Tat circuit does not establish bistability through other mechanisms (e.g., nonlinear degradation), we tested for hysteresis in a minimal Tat-LTR feedback circuit, where LTR drives expression of an unstable (2 h half-life) GFP reporter (d2GFP) and an internal ribosome entry site enables coexpression of Tat fused

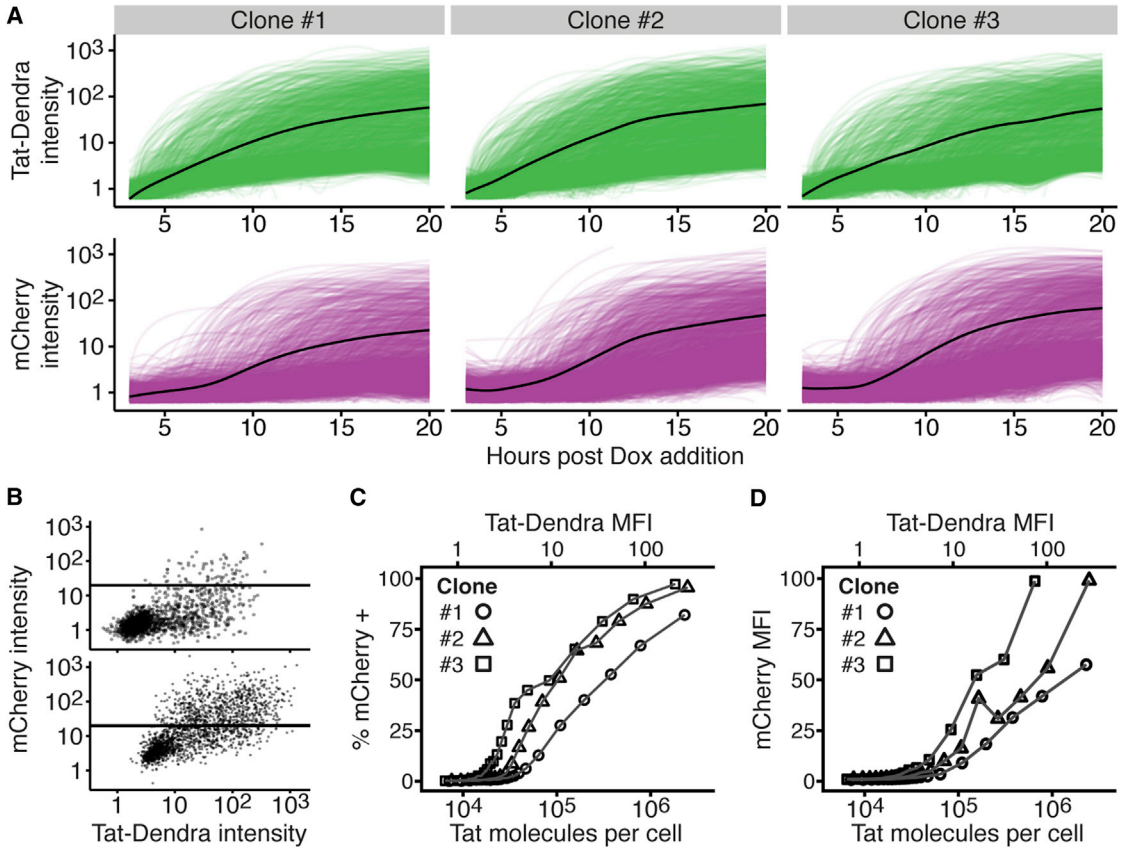

FIGURE 3 Time-lapse microscopy verifies that the LTR exhibits an activation threshold at early times. (*A*) Given here is time-lapse fluorescence microscopy imaging of single cells from three Jurkat cell isoclonal populations each encoding both Tat-Dendra and LTR-mCherry-deg. Cells were activated and then imaged for 20 h. Tat-Dendra trajectories are green; mCherry trajectories are magenta; mean intensity trace shown in black. Approximately two-thousand cell trajectories are shown for each clone. (*B*) Given here is a flow-style dot plot of Tat-Dendra versus mCherry intensities from time-lapse images at $t = 10$ h (*upper*) and $t = 20$ h (*lower*) of Clone #2. Each dot represents an individual cell. As in Fig. 2, the horizontal line marks the mCherry-positive cutoff gate. (*C* and *D*) Given here are dose-response curves for % of mCherry + cells (*left*) and mCherry MFI versus Tat MFI and calculated number of Tat molecules per cell. Single-cell intensities extracted from all images were pooled and processed in the same manner as the flow data (each *point* summarizes 10^4 observations). Tat-Dendra signal intensity was converted to molecular number using a GFP molecular ruler.

to the tunable proteolysis tag FKBP (Fig. 1 *C*). In this circuit (hereafter "Ld2GITF"), Tat proteolysis can be protected by the small molecule Shield-1 (44), thereby allowing feedback strength to be tuned (26) and alternate paths of the circuit—ON-to-OFF versus OFF-to-ON—to be examined. Specifically, cells in the GFP ON state (i.e., preincubated in Shield-1) can be exposed to successively decreasing Shield-1 levels to examine turning OFF of the circuit, whereas cells in the GFP OFF state (i.e., no Shield-1 preincubation) can be exposed to successively increasing Shield-1 levels to examine turning ON of the circuit. The difference (Δ) in percentage of GFP ON cells for a specific Shield-1 concentration can be quantified, with $\Delta > 1$ indicating hysteresis. If hysteresis is present, cells beginning in the ON state (i.e., pretreated with high Shield-1) will be more likely to remain ON at a specific intermediate dose of Shield-1, as compared to cells that began in the OFF state (i.e., non-pretreated cells); whereas, if hysteresis is not present ($\Delta = 1$), there will no difference in ON-OFF percentages for cells beginning in either the ON or OFF state. We tested five isoclonal Ld2GITF populations carrying single integrations of the Ld2GITF circuit, and measured Δ to be ≈ 1 (mean, 1.008; 95% CI, 0.813–1.203; Fig. 1 *D*), indicating that hysteresis is unlikely. These hysteresis measurements build upon previous data indicating that the necessary conditions for deterministic bistability are absent in the HIV Tat-LTR circuit (32).

Single-cell flow cytometry analysis of the HIV LTR-Tat dose-response function shows a thresholdlike response that is transient in time

Absent bistability, it was unclear how the Tat-LTR circuit might encode a threshold to temporarily remain OFF to provide an opportunity for the kinetically slower epigenetic-silencing mechanisms to act. Importantly, chromatin-silencing mechanisms appear unable to silence the actively transcribing promoter (26).

First, to check if the Tat-LTR circuit encodes an activation threshold, we directly quantified LTR activity as a function of Tat levels using an open-loop Tat-LTR dose-response system. In this system, one construct encodes Tat fused to the fluorescent reporter Dendra2 expressed from a doxycycline-inducible tet promoter, whereas a second construct encodes an mCherry reporter expressed from the LTR promoter (Fig. 2 *A*). This open-loop system allows Tat levels to be tuned by Dox and enables both Tat (dose) levels and LTR (response) levels to be quantified in the same cell (26) so that the dose-response transfer function for Tat and LTR can be fit and an effective Hill coefficient calculated.

To estimate the conditional probability of LTR mean expression level and percentage ON for a given Tat level from flow cytometry data, a binning method similar to previous methods (45) was used (Fig. 2, *B* and *C*). Examination of the flow cytometry time-course data showed that the LTR appears essentially nonresponsive to Tat at low Tat levels, but LTR activity then increases sharply over a narrow range of Tat (Fig. 2 *D*). At early times after Dox activation, a pronounced shoulder is visible in Tat expression where a substantial percentage of cells express Tat-Dendra, but these cells do not express mCherry from the LTR. This delay between Tat-Dendra and mCherry expression is on the order of 8–12 h, which is too long to simply be a temporal delay in expression of mCherry due to activation by Tat-Dendra.

For all LTR isoclones (i.e., integration sites) examined, the dose-response expression curves for mCherry mean expression and percentage of mCherry ON cells exhibit a conspicuous activation threshold (Fig. 2 *E*). The LTR appears essentially nonresponsive to Tat at low Tat levels, but LTR activity then increases sharply over a narrow range of Tat. This thresholding behavior appears to be maximized at intermediate time points of 16–20 h (Fig. 2, *F* and *G*). At early times, the response is incomplete, but by 40 h, the dose-response curves flatten with the K_{50} shifting to lower Tat expression.

Time-lapse microscopy analysis verifies the thresholdlike LTR response to Tat at early times after activation

To verify that this result was not simply a peculiarity of the flow cytometry approach, we next examined activation of this open-loop activation circuit using quantitative time-lapse imaging (Fig. 3 *A*). Jurkat isoclones, as above, were imaged for 20 h after Dox activation, and for all isoclones, there was a conspicuous delay of $\sim$7 h in mCherry expression relative to Tat-Dendra expression (Fig. 3, *A* and *B*). The single-cell trajectories were then used to construct Tat-LTR dose-response trajectories via the same conditional binning method as used for flow cytometry (Supporting Material). For all LTR isoclones examined, the dose-response expression curves for both mCherry mean expression and percentage of mCherry ON cells exhibits a conspicuous activation threshold (Fig. 3, *C* and *D*). As observed in flow cytometry, the microscopy imaging shows that the LTR is essentially nonresponsive to Tat at low Tat levels, but LTR activity then increases sharply over a narrow range of Tat.

We used a molecular-ruler approach (36,37) to convert Tat-Dendra fluorescence levels to molecular number (Materials and Methods; Supporting Material). For all clones tested, the threshold level of Tat proteins required to minimally activate the LTR (i.e., >2% mCherrypositive cells) is in the tens of thousands of molecules, with the average being 4.4×10^4 Tat/cell (Fig. 3, *C* and *D*). Comparable values for Tat molecules per cell were previously obtained in a minimal Tat-LTR feedback circuit, with quantitation performed by GFP standard beads (46). Upon accounting for cell size differences, this molecular threshold value was also not dissimilar to those calculated for phage-λ, where 55 Cro molecules are required for lytic infection and

145 CI molecules are required for lysogeny (13); human lymphocytes are $\sim 10^3$ times the volume of *E. coli* (47).

Transcriptional activation by TNF effectively accelerates the transient lifetime of the LTR activation threshold

Based on observations that HIV latency can be partially reversed by transcriptional activators, we next asked if transcriptional activators could alter the observed LTR-activation threshold. To transcriptionally activate the LTR, we used the well-characterized cytokine TNFα, which acts through nuclear factor kappa B (NF-κB) signaling to recruit transcriptional activators to the LTR (26,48,49), thereby increasing LTR transcriptional burst frequency (33,42,50).

When the dose-response function is measured post-Dox induction in the presence of TNF, the response functions show both a marked shortening of the lifetime of the threshold and a reduced threshold (Fig. 4 *A*; Figs. S5 and S6). In fact, when comparing the dose-responses in the presence and absence of TNF, the presence of TNF caused the 20-h dose-response curve to look similar to the 40-h non-TNF dose-response curves (compare Fig. 4 *A* to Fig. 2 *E*). Consistent with this observation, the calculated Hill coefficients, expressed as H, decreases in the presence of TNF (Fig. 4 *B*) and, with the exception of Clone #2's mean fluorescence intensity (MFI), the K_{50} values decline in the presence of TNF (Fig. 4 *C*), indicating that the threshold becomes progressively weaker.

A minimal stochastic model is sufficient to recapitulate the transient-threshold effect

We next explored whether a mechanistic model could be developed to explain the transient threshold effect. Given the lack of bistability (32) and hysteresis in the circuit (Fig. 1), we neglected models that postulated built-in cooperative responses or deterministic thresholds (i.e., models with a deterministic $H > 1$).

Based on previous literature on ultrasensitive threshold responses (19), we first examined a set of deterministic ODE models (Supporting Material) that are noncooperative (i.e., $H = 1$) but have architectures found in ultrasensitive responses, namely enzymatic interconversions in the zero-order regime. In these models, Tat is reversibly covalently modified—acetylated at lysine residues by p300 and deacetylated by SirT1, with acetylation required for efficient transactivation of the LTR but deacetylation being more rapid than acetylation (32,51). The rationale for testing these models was that the Tat-Dendra reporter (Fig. 2)

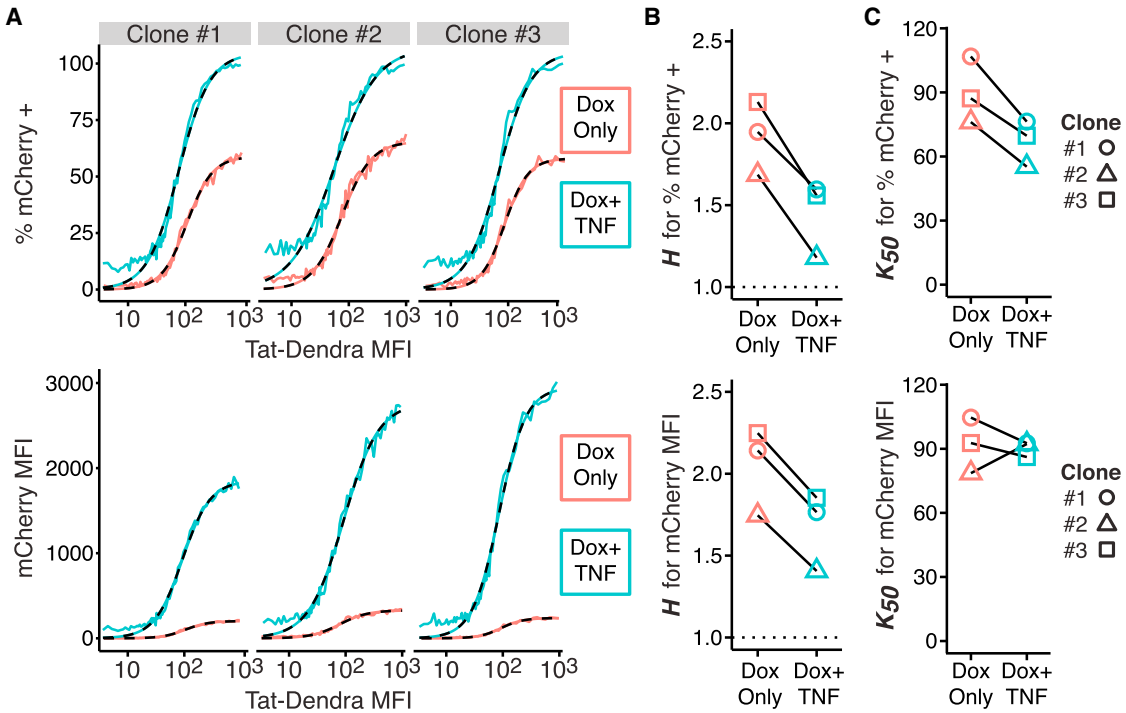

FIGURE 4 Transcriptional activation by TNF effectively accelerates the transient lifetime of the LTR activation threshold. (*A*) Given here are dose-response curves for % of mCherry-positive cells (*top*) and mCherry MFI (*bottom*) from flow cytometry measurements of three isoclones of Jurkat Tet-Tat-Dendra + LTR-mCherry, at 20 h post-Dox induction in the presence or absence of TNF. Each data point depicts a group of 500 cells. These data were fit to a Hill function (*dashed lines*); numeric results are given in Fig. S6. (*B*) Given here are Hill coefficients, H, determined from dose-response curve fitting, demonstrating empirical positive cooperativity ($H > 1$) with lowering of H-values for cells treated with TNF. The expected noncooperative response is indicated by the dotted line at $H = 1$. (*C*) Given here is half-maximal response (K_{50}), determined from dose-response curve fitting.

does not distinguish between acetylated and deacetylated Tat and most Tat in the cell is deacetylated (32,51), so Dendra intensity primarily quantifies Tat that is not transactivating the LTR. Moreover, given the faster deacetylation rate, a large amount of deacetylated Tat protein is required for significant acetylated Tat to be present. Nevertheless, in the deterministic regime, models of this form do not generate threshold responses either at steady state or in the pre-steady-state transient regime (Supporting Material). This is because—without postulating an ad hoc threshold for Tat acetylation—the continuous nature of deterministic ODEs results in a small fractional value of Tat protein being continuously acetylated and thus being transactivation competent.

Given the continuous nature of ODE models, we next examined minimal stochastic chemical reaction (master equation) models as these models account for integer molecule numbers. These models intrinsically form a threshold because a single molecule of active transactivator (rather than a continuous fractional value) is required for a reaction to occur. As above, we hypothesized that the rates of conversion from the inactive to the active state could allow many transactivator molecules to be transiently present in the inactive state before a single molecule of active transactivator (acetylated Tat) is produced, thereby establishing a transient threshold. To test this hypothesis, four stochastic models of increasing complexity were built (models *i–iv*; see Table 1).

The models are presented using a generic nomenclature where the active transcription factor (TF) represents Tat; the TF can be in an inactive form (TF_i) requiring a single modification to become active TF, or (TF_{ii}) requiring two modifications to become active TF. The promoter, which represents the LTR, can toggle between an on-state (Pr_{on}) or off-state (Pr_{off}). For computational expediency and simplicity, the models are coarse grained to neglect the mRNA intermediate. Models *i–iv* were then numerically simulated for the LTR-Tat system (TF = Tat-Dendra, *Pr* = LTR, *Protein* = mCherry, and $k_\propto$ is Dox induction; (Fig. 5)). In model *i*, active TF is produced at linear rate $k_\propto$, transactivates Pr_{on} by forming the [TF_Pr_{on}] complex and, as expected, generates linear dose-responses for Protein (mCherry) as a function of TF (Tat-Dendra) (Fig. 5). When the model is extended (model *ii*) so that TF is produced as inactive and reversibly modified to active ($TF_i \leftrightarrow TF$), a slight threshold in dose response appears at early times (Fig. 5). The lifetime of this transient threshold is extended by inclusion of promoter toggling (model *iii*) and further extended (model *iv*) by additional transactivator toggling reactions ($TF_{ii} \leftrightarrow TF_i \leftrightarrow TF$) (Fig. 5).

One prediction of these models (Fig. 5) is that accelerating the promoter toggling transition from Pr_{off} to Pr_{on} (increasing k_{on}) should shorten the transient lifetime (for the extreme case: compare models *iii/iv* to model *ii* in Fig. 5 where $k_{on} \rightarrow \infty$). In support of this, TNF induction increases k_{on} for the LTR (33,42), and the data in Fig. 4 show that TNF substantially shortens the lifetime of the transient threshold.

TABLE 1 Reaction Schemes for Stochastic Models Simulated in Figure 5

Model *i*	Model *ii*	Model *iii*	Model *iv*
$\varnothing \xrightarrow{k_\propto} TF$	$\varnothing \xrightarrow{k_\propto} TF_i$	$\varnothing \xrightarrow{k_\propto} TF_i$	$\varnothing \xrightarrow{k_\propto} TF_{ii}$
	$TF_i \xrightarrow{k_a} TF$	$TF_i \xrightarrow{k_a} TF$	$TF_{ii} \xrightarrow{k_a} TF_i$
	$TF \xrightarrow{k_i} TF_i$	$TF \xrightarrow{k_i} TF_i$	$TF_i \xrightarrow{k_i} TF_{ii}$
		$Pr_{OFF} \xrightarrow{k_{on}} Pr_{ON}$	$TF_i \xrightarrow{k_a} TF$
		$Pr_{ON} \xrightarrow{k_{off}} Pr_{OFF}$	$TF \xrightarrow{k_i} TF_i$
			$Pr_{OFF} \xrightarrow{k_{on}} Pr_{ON}$
			$Pr_{ON} \xrightarrow{k_{off}} Pr_{OFF}$

All models (*i–iv*) also include the following common reactions: $TF + Pr_{ON} \underset{k_r}{\overset{k_f}{\rightleftarrows}} [TF\_Pr_{ON}] \xrightarrow{k_{transact}} TF + Pr_{ON} + \text{Protein}$; $\text{Protein} \xrightarrow{\gamma} \varnothing$; and $TF \xrightarrow{\gamma 2} \varnothing$ (TF_i and TF_{ii} also decay at rate $\gamma 2$).

DISCUSSION

HIV's ability to establish latency in resting $CD4^+$ T lymphocytes remains the chief barrier to curative therapy (22) and an area of active study. Latency establishment does not correlate with viral integration site (23–25) or progressive cellular silencing, and the Tat positive-feedback circuit is necessary and sufficient for latency establishment (26), with epigenetic chromatin silencing possibly maintaining the latent state (31). However, given the noncooperative nature of Tat feedback (32), the circuit was thought to lack an activation threshold, and so it was unclear how HIV could even temporarily remain in an off-state to provide an opportunity for the kinetically slower epigenetic silencing mechanisms to act and stabilize latency.

Here, using combination of single-cell analyses (flow cytometry and time-lapse microscopy), we find that the HIV Tat circuit exhibits a transient threshold in activation that disappears over time (Figs. 2 and 3). Promoter activation by TNF shortens the lifetime of this transient threshold (Fig. 4). The transient nature of the threshold accounts for the lack of deterministic bistability and hysteresis in the circuit and previous findings that Tat feedback is noncooperative (32). We find that a stochastic model, combining two previous models (32,42), where the transcriptional transactivator and promoter both toggle between active and inactive states, qualitatively recapitulates the transient-threshold effect (Fig. 5). Other models with additional promoter states (e.g., three-state LTR models) would likely also recapitulate the effect (52).

At its core, the stochastic model generates this threshold—whereas continuous ODE models do not—because the stochastic model accounts for integer numbers of TF molecules. Thus, the stochastic model intrinsically forms a threshold by requiring a single molecule of acetylated Tat (active TF), rather than a continuous fractional value. Due to rates of conversion, excess molecules are

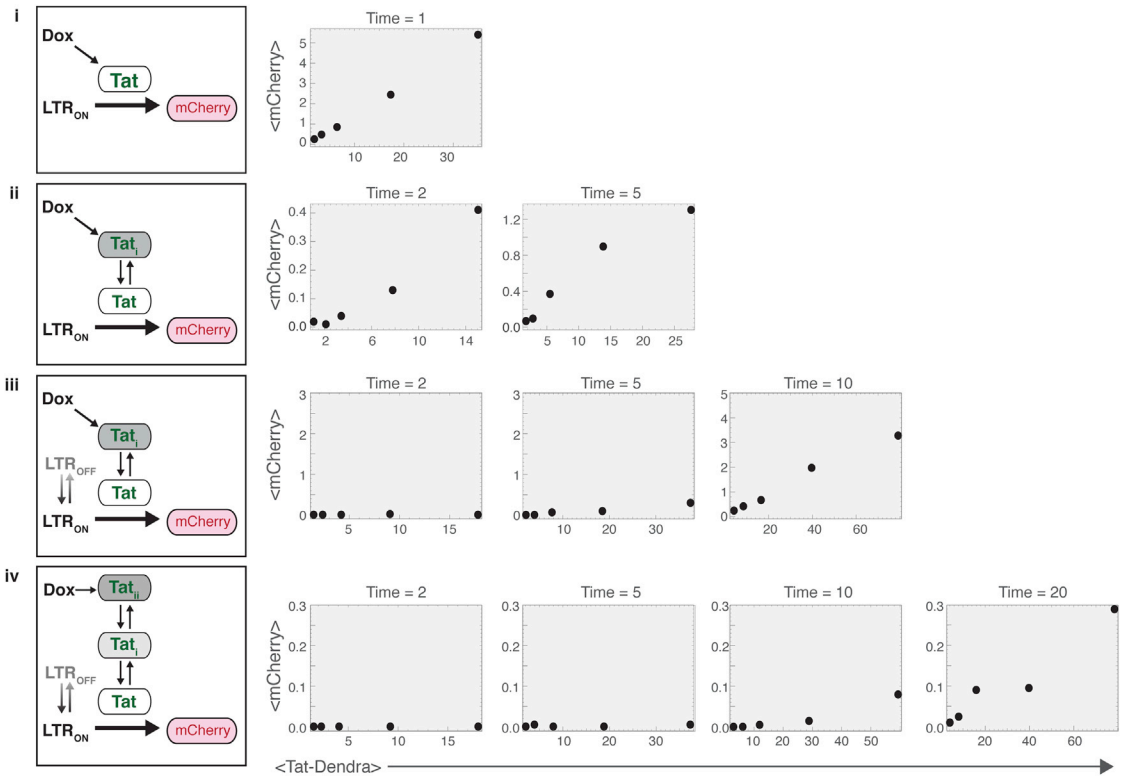

FIGURE 5 Stochastic models where the transactivator and promoter toggle between active and inactive qualitatively recapitulate the transient dose-response threshold. (*Left*) Shown here are schematics of models (*i–iv*) for the LTR-Tat system (i.e., $TF = Tat$, $Pr = LTR$, $Protein = mCherry$, and k_a is *Dox* induction). In all models, Tat is generated from the Dox-inducible promoter (at rate $k_\propto$), and mCherry is driven from the LTR. (*Right*) Shown here are corresponding dose-response functions from stochastic simulations. Mean mCherry and mean Tat-Dendra calculated from 200 simulation runs at each specified time point (arbitrary time units). Both active transactivator (*Tat*) and inactive transactivator (Tat_i and Tat_{ii}) are Dendra labeled; reverse reactions (e.g., $LTR_{OFF} \rightarrow LTR_{ON}$ and $Tat \rightarrow Tat_i$) are 10-fold faster than forward reaction rates. (*i*) Given here is a model where neither the promoter toggles (only LTR_{ON}) nor the transactivator toggles (only Tat), and exhibit a linear dose response of mCherry to Tat even at early times; (*ii*) a model where the transactivator is produced as inactive but is then converted to active (i.e., only the transactivator toggles: $Tat \leftrightarrow Tat_i$), and exhibits a slight threshold in dose response at early times; (*iii*) a model where both the transactivator and promoter toggle ($LTR_{OFF} \leftrightarrow LTR_{ON}$ and $Tat \leftrightarrow Tat_i$), and extends the transient threshold; and (*iv*) a model where the promoter toggles ($LTR_{OFF} \leftrightarrow LTR_{ON}$) and the transactivator toggles between three forms ($Tat_{ii} \leftrightarrow Tat_i \leftrightarrow Tat$), further extending the transient threshold lifetime. Parameter values used were: {$k_\propto$ varied [0.5–10] to generate different Tat-Dendra levels, $k_a = 0.05$, $k_i = 0.5$, $\gamma = \gamma^2 = 0.1$, $k_{off} = 0.5$, $k_{on} = 0.1$, $k_f = k_r = 0.5$} and all initial conditions were set to zero (except $LTR_{OFF} = 1$).

transiently present in the inactive state before a single molecule appears in the active state, thereby establishing a transient threshold. This effect is interesting to contrast with the other effects of stochasticity in ultrasensitive systems (53).

Physiologically, the transient nature of the threshold may allow the Tat circuit to temporarily remain in an off-state and buffer stochastic fluctuations from rapidly triggering positive feedback and active replication, thereby providing a temporal window for the kinetically slower epigenetic silencing mechanisms to stabilize the off-state. Given the widespread nature of promoter toggling and transcription factor modifications, transient thresholds may be a general feature of inducible promoters.

One caveat to our study is that we only examined a small number of isoclonal integration sites for the LTR promoter. It is possible that these integration sites are somehow unique in their ability to generate a threshold and that higher-throughput analyses of integration sites will produce a different result. It is also important to note that different integration sites yield different effective Hill coefficients (Fig. 2 *E*) and given this range of Hill coefficients, additional integration sites should be analyzed to establish whether the circuit in fact exhibits $H > 1$. If indeed $H > 1$, the model would need to generate a probability of the system being in the active promoter complex [TF_Pr_{on}] that scales with hyperbolic curvature as a function of TF; more formally, there must be some nonzero value of TF where $\partial^2[P(TF\_Pr_{on})]/\partial[TF]^2 = 0$. However, in models *i–iv*, it is straightforward to algebraically show that $\partial^2[P(TF\_Pr_{on})]/\partial[TF]^2 \neq 0$ for any nonzero value of TF.

To transiently generate $H > 1$, some form of TF cooperativity is required. This cooperativity could in principle be achieved through homomultimerization (1,20,54) of the TF protein, or successive covalent modifications (55) of TF, or successive TF-dependent steps required for promoter activation. However, to recapitulate the data, it is absolutely

critical that the mechanism of cooperativity be transient and disappear over time (or disappear as TF levels increase). The homomultimerization mechanism is the most difficult to reconcile with this. Although the active form of Tat might multimerize at early times (low levels of Tat) but then become a monomer at later times (high Tat levels) or under TNF stimulation, this scenario would be an exotic departure from the typical biophysical models of concentration-dependent multimerization of a protein (i.e., monomeric at low concentrations with crowding-induced multimerization). In contrast, it may be more appealing to consider models where at early times (low Tat or LTR-expression levels) two successive Tat-dependent steps are required for LTR activation but as the promoter increases in transcriptional activity, one of these Tat-dependent steps becomes a Tat-independent step. For example, active and quiescent promoters differentially localize in the nucleus (56,57), and if the genomic locus where the LTR integrates repositions as LTR activity increases, the LTR may be subject to different activation signals when it reaches a new nuclear microenvironment (58). In other words, at early times during activation, the LTR locus is in a quiescent nuclear microenvironment, whereas at later times after activation, the LTR may reposition to a more TNF-like nuclear microenvironment.

There may also exist additional thresholds in LTR activation, such as in response to chromatin remodeling (59). However, as discussed above, the epigenetic chromatin-silencing mechanisms that allow for chromatin-mediated reactivation are dynamically slower effects that cannot explain establishment of latency (26), and thus, this chromatin threshold is likely distinct from the early time transient thresholding results observed here.

Regarding the potential benefits of such transient thresholding relative to multistability, we can only provide speculation. When molecular thresholds are established through self-cooperativity and multistability, it is biochemically difficult to alter the threshold level. In the case of the Tat-LTR circuit, TNF (Fig. 4) and other cellular activators (e.g., TSA; Fig. S6) can alter the threshold. Future work will focus on validating the proposed molecular mechanisms (Fig. 5) that establish the transient threshold and its tunability.

SUPPORTING MATERIAL

Supporting Materials and Methods and six figures are available at http://www.biophysj.org/biophysj/supplemental/S0006-3495(17)30503-9.

AUTHOR CONTRIBUTIONS

K.H.A. and L.S.W. designed the research. K.H.A. and E.J.T. performed the research. K.H.A., E.J.T., M.T., and L.S.W. analyzed data. K.H.A., M.T., and L.S.W. wrote the paper.

ACKNOWLEDGMENTS

We thank Brandon Razooky for key initial observations and reagents, and Marielle Cavrois of the Gladstone Institutes Flow Cytometry Core and Kurt Thorn of the University of California San Francisco Nikon Imaging Center for technical help and advice.

The Gladstone Institutes Flow Cytometry Core is supported by National Institutes of Health (NIH) grant Nos. P30 AI027763 and S10 RR028962. K.H.A. was supported by a National Science Foundation (NSF) Graduate Research Fellowship. M.T. acknowledges support from the National Institutes of Health (NIH) Office of the Director, the National Cancer Institute, and the National Institute of Dental and Craniofacial Research under NIH grant No. DP5 OD012194. L.S.W. acknowledges support from the NIH Director's New Innovator Award Program, grant No. OD006677, and NIH grant No. R01 AI109593.

REFERENCES

1. Wall, M. E., W. S. Hlavacek, and M. A. Savageau. 2004. Design of gene circuits: lessons from bacteria. *Nat. Rev. Genet.* 5:34–42.
2. Alon, U. 2007. Network motifs: theory and experimental approaches. *Nat. Rev. Genet.* 8:450–461.
3. Gunawardena, J. 2005. Multisite protein phosphorylation makes a good threshold but can be a poor switch. *Proc. Natl. Acad. Sci. USA.* 102:14617–14622.
4. Ferrell, J. E., Jr. 2002. Self-perpetuating states in signal transduction: positive feedback, double-negative feedback and bistability. *Curr. Opin. Cell Biol.* 14:140–148.
5. Das, J., M. Ho, …, J. P. Roose. 2009. Digital signaling and hysteresis characterize ras activation in lymphoid cells. *Cell.* 136:337–351.
6. Strogatz, S. H. 2014. Nonlinear Dynamics and Chaos: with Applications to Physics, Biology, Chemistry, and Engineering. Westview, Boulder, CO.
7. Melen, G. J., S. Levy, N. Barkai, and B.-Z. Shilo. 2005. Threshold responses to morphogen gradients by zero-order ultrasensitivity. *Mol. Syst. Biol.* 1:2005.0028.
8. Goldbeter, A., and D. E. Koshland, Jr. 1981. An amplified sensitivity arising from covalent modification in biological systems. *Proc. Natl. Acad. Sci. USA.* 78:6840–6844.
9. Mitrophanov, A. Y., and E. A. Groisman. 2008. Positive feedback in cellular control systems. *BioEssays.* 30:542–555.
10. Losick, R., and C. Desplan. 2008. Stochasticity and cell fate. *Science.* 320:65–68.
11. Gardner, T. S., C. R. Cantor, and J. J. Collins. 2000. Construction of a genetic toggle switch in *Escherichia coli*. *Nature.* 403:339–342.
12. Bednarz, M., J. A. Halliday, …, I. Golding. 2014. Revisiting bistability in the lysis/lysogeny circuit of bacteriophage λ. *PLoS One.* 9:e100876.
13. Arkin, A., J. Ross, and H. H. McAdams. 1998. Stochastic kinetic analysis of developmental pathway bifurcation in phage λ-infected *Escherichia coli* cells. *Genetics.* 149:1633–1648.
14. Ozbudak, E. M., M. Thattai, …, A. Van Oudenaarden. 2004. Multistability in the lactose utilization network of *Escherichia coli*. *Nature.* 427:737–740.
15. Süel, G. M., J. Garcia-Ojalvo, …, M. B. Elowitz. 2006. An excitable gene regulatory circuit induces transient cellular differentiation. *Nature.* 440:545–550.
16. Maamar, H., and D. Dubnau. 2005. Bistability in the *Bacillus subtilis* K-state (competence) system requires a positive feedback loop. *Mol. Microbiol.* 56:615–624.
17. Levine, E., Z. Zhang, …, T. Hwa. 2007. Quantitative characteristics of gene regulation by small RNA. *PLoS Biol.* 5:e229.
18. Chen, D., and A. P. Arkin. 2012. Sequestration-based bistability enables tuning of the switching boundaries and design of a latch. *Mol. Syst. Biol.* 8:620.

19. Ferrell, J. E., Jr., and S. H. Ha. 2014. Ultrasensitivity part I: Michaelian responses and zero-order ultrasensitivity. *Trends Biochem. Sci.* 39: 496–503.
20. Dill, K., and S. Bromberg. 2010. Molecular Driving Forces: Statistical Thermodynamics in Biology, Chemistry, Physics, and Nanoscience. Garland Science, New York.
21. Weinberger, L. S. 2015. A minimal fate-selection switch. *Curr. Opin. Cell Biol.* 37:111–118.
22. Richman, D. D., D. M. Margolis, …, R. J. Pomerantz. 2009. The challenge of finding a cure for HIV infection. *Science.* 323:1304–1307.
23. Ho, Y.-C., L. Shan, …, R. F. Siliciano. 2013. Replication-competent noninduced proviruses in the latent reservoir increase barrier to HIV-1 cure. *Cell.* 155:540–551.
24. Sherrill-Mix, S., M. K. Lewinski, …, F. D. Bushman. 2013. HIV latency and integration site placement in five cell-based models. *Retrovirology.* 10:90.
25. Lewinski, M. K., D. Bisgrove, …, F. D. Bushman. 2005. Genome-wide analysis of chromosomal features repressing human immunodeficiency virus transcription. *J. Virol.* 79:6610–6619.
26. Razooky, B. S., A. Pai, …, L. S. Weinberger. 2015. A hardwired HIV latency program. *Cell.* 160:990–1001.
27. Tyagi, M., R. J. Pearson, and J. Karn. 2010. Establishment of HIV latency in primary CD^{4+} cells is due to epigenetic transcriptional silencing and P-TEFb restriction. *J. Virol.* 84:6425–6437.
28. Calvanese, V., L. Chavez, …, E. Verdin. 2013. Dual-color HIV reporters trace a population of latently infected cells and enable their purification. *Virology.* 446:283–292.
29. Dahabieh, M. S., M. Ooms, …, I. Sadowski. 2013. A doubly fluorescent HIV-1 reporter shows that the majority of integrated HIV-1 is latent shortly after infection. *J. Virol.* 87:4716–4727.
30. Whitney, J. B., A. L. Hill, …, D. H. Barouch. 2014. Rapid seeding of the viral reservoir prior to SIV viraemia in rhesus monkeys. *Nature.* 512:74–77.
31. Siliciano, R. F., and W. C. Greene. 2011. HIV latency. *Cold Spring Harb. Perspect. Med.* 1:a007096.
32. Weinberger, L. S., and T. Shenk. 2007. An HIV feedback resistor: auto-regulatory circuit deactivator and noise buffer. *PLoS Biol.* 5:e9.
33. Dar, R. D., B. S. Razooky, …, L. S. Weinberger. 2012. Transcriptional burst frequency and burst size are equally modulated across the human genome. *Proc. Natl. Acad. Sci. USA.* 109:17454–17459.
34. Dey, S. S., J. E. Foley, …, A. P. Arkin. 2015. Orthogonal control of expression mean and variance by epigenetic features at different genomic loci. *Mol. Syst. Biol.* 11:806.
35. Perelson, A. S., A. U. Neumann, …, D. D. Ho. 1996. HIV-1 dynamics in vivo: virion clearance rate, infected cell life-span, and viral generation time. *Science.* 271:1582–1586.
36. Charpilienne, A., M. Nejmeddine, …, J. Cohen. 2001. Individual rotavirus-like particles containing 120 molecules of fluorescent protein are visible in living cells. *J. Biol. Chem.* 276:29361–29367.
37. Desai, P., and S. Person. 1998. Incorporation of the green fluorescent protein into the herpes simplex virus type 1 capsid. *J. Virol.* 72:7563–7568.
38. Gibson, W. 1996. Structure and assembly of the virion. *Intervirology.* 39:389–400.
39. Chudakov, D. M., S. Lukyanov, and K. A. Lukyanov. 2007. Tracking intracellular protein movements using photoswitchable fluorescent proteins PS-CFP2 and Dendra2. *Nat. Protoc.* 2:2024–2032.
40. Dar, R. D., N. N. Hosmane, …, L. S. Weinberger. 2014. Screening for noise in gene expression identifies drug synergies. *Science.* 344:1392–1396.
41. Singh, A., B. S. Razooky, …, L. S. Weinberger. 2012. Dynamics of protein noise can distinguish between alternate sources of gene-expression variability. *Mol. Syst. Biol.* 8:607.
42. Singh, A., B. Razooky, …, L. S. Weinberger. 2010. Transcriptional bursting from the HIV-1 promoter is a significant source of stochastic noise in HIV-1 gene expression. *Biophys. J.* 98:L32–L34.
43. Gillespie, D. T. 1977. Exact stochastic simulation of coupled chemical-reactions. *J. Phys. Chem.* 81:2340–2361.
44. Banaszynski, L. A., L.-C. Chen, …, T. J. Wandless. 2006. A rapid, reversible, and tunable method to regulate protein function in living cells using synthetic small molecules. *Cell.* 126:995–1004.
45. Krishnaswamy, S., M. H. Spitzer, …, G. P. Nolan. 2014. Systems biology. Conditional density-based analysis of T cell signaling in single-cell data. *Science.* 346:1250689.
46. Weinberger, L. S., J. C. Burnett, …, D. V. Schaffer. 2005. Stochastic gene expression in a lentiviral positive-feedback loop: HIV-1 Tat fluctuations drive phenotypic diversity. *Cell.* 122:169–182.
47. Milo, R., P. Jorgensen, …, M. Springer. 2010. BioNumbers—the database of key numbers in molecular and cell biology. *Nucleic Acids Res.* 38:D750–D753.
48. Jordan, A., P. Defechereux, and E. Verdin. 2001. The site of HIV-1 integration in the human genome determines basal transcriptional activity and response to Tat transactivation. *EMBO J.* 20:1726–1738.
49. Jordan, A., D. Bisgrove, and E. Verdin. 2003. HIV reproducibly establishes a latent infection after acute infection of T cells in vitro. *EMBO J.* 22:1868–1877.
50. Dar, R. D., S. M. Shaffer, …, L. S. Weinberger. 2016. Transcriptional bursting explains the noise-versus-mean relationship in mRNA and protein levels. *PLoS One.* 11:e0158298.
51. Pagans, S., A. Pedal, …, M. Ott. 2005. SIRT1 regulates HIV transcription via Tat deacetylation. *PLoS Biol.* 3:e41.
52. Chavali, A. K., V. C. Wong, and K. Miller-Jensen. 2015. Distinct promoter activation mechanisms modulate noise-driven HIV gene expression. *Sci. Rep.* 5:17661.
53. Berg, O. G., J. Paulsson, and M. Ehrenberg. 2000. Fluctuations and quality of control in biological cells: zero-order ultrasensitivity reinvestigated. *Biophys. J.* 79:1228–1236.
54. Teng, M. W., C. Bolovan-Fritts, …, L. S. Weinberger. 2012. An endogenous accelerator for viral gene expression confers a fitness advantage. *Cell.* 151:1569–1580.
55. Ferrell, J. E., Jr., and E. M. Machleder. 1998. The biochemical basis of an all-or-none cell fate switch in *Xenopus* oocytes. *Science.* 280: 895–898.
56. Simonis, M., P. Klous, …, W. de Laat. 2006. Nuclear organization of active and inactive chromatin domains uncovered by chromosome conformation capture-on-chip (4C). *Nat. Genet.* 38:1348–1354.
57. Cavalli, G., and T. Misteli. 2013. Functional implications of genome topology. *Nat. Struct. Mol. Biol.* 20:290–299.
58. Lusic, M., B. Marini, …, M. Giacca. 2013. Proximity to PML nuclear bodies regulates HIV-1 latency in CD^{4+} T cells. *Cell Host Microbe.* 13:665–677.
59. Miller-Jensen, K., S. S. Dey, …, D. V. Schaffer. 2012. Chromatin accessibility at the HIV LTR promoter sets a threshold for NF-κB mediated viral gene expression. *Integr. Biol.* 4:661–671.

Biophysical Journal, Volume *112*

Supplemental Information

Transient Thresholding: A Mechanism Enabling Noncooperative Transcriptional Circuitry to Form a Switch

Katherine H. Aull, Elizabeth J. Tanner, Matthew Thomson, and Leor S. Weinberger

Supporting Material

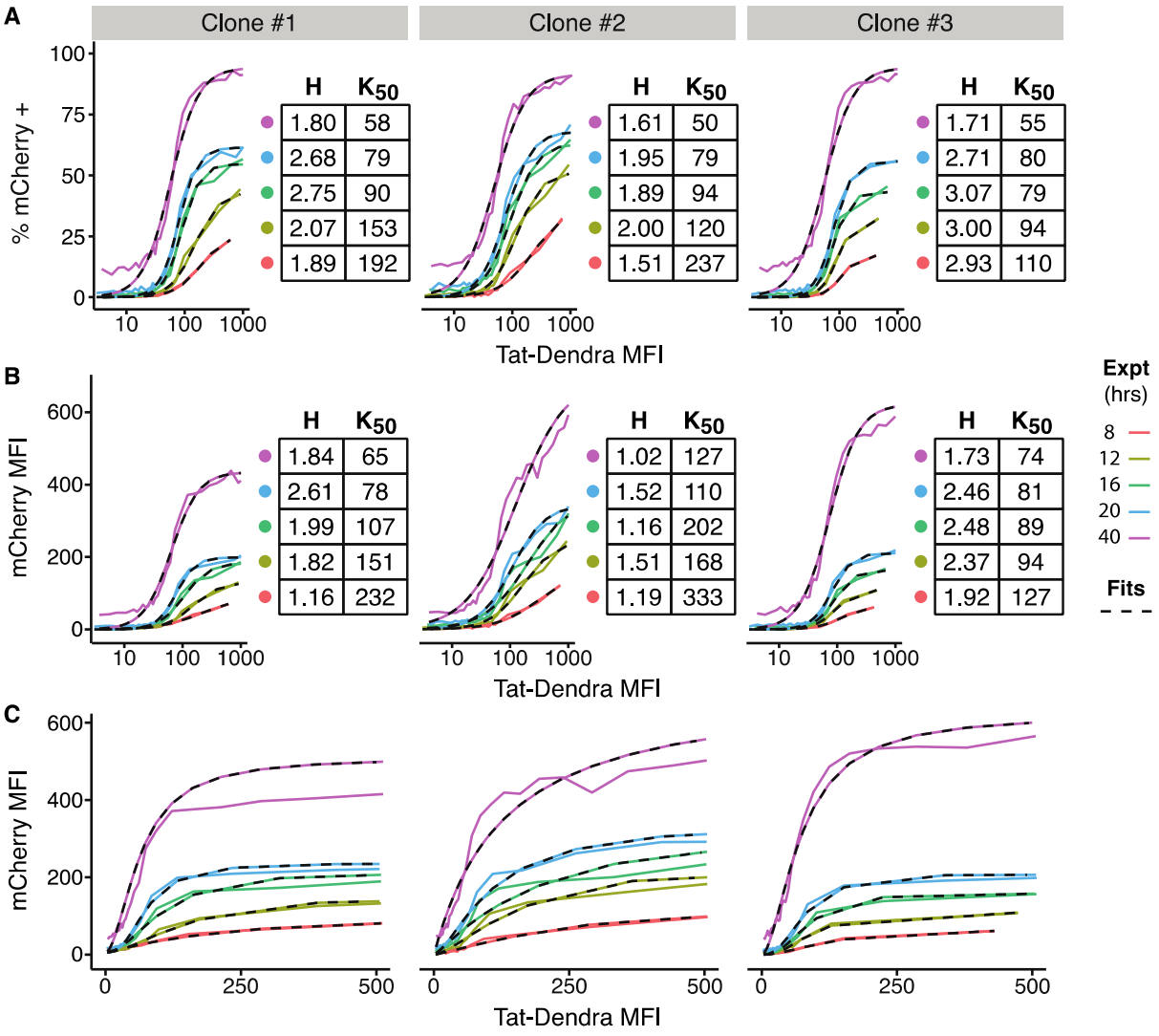

Figure S1: The open-loop Tat-LTR circuit exhibits a threshold in both activation and mean expression. (A) Flow data from three isoclones of Jurkat Tat-Dendra + LTR mCherry-deg cells, as shown in raw form in Fig. 2D and as dose-response plots in Fig. 2E, fit to a Hill function (Methods). The dose-response data and Hill fit lines are depicted for each condition, with Hill coefficient (*H*) and half-maximal binding (K_{50}) values in adjacent tables together with goodness of fit (R^2). (B) The equivalent dose-mean expression curves in Fig. 2E were analyzed as in panel A. (C) Data and fits from panel B, with Tat-Dendra on a linear scale to emphasize the weakly sigmoidal shape. All fits gave $R^2 > 0.96$.

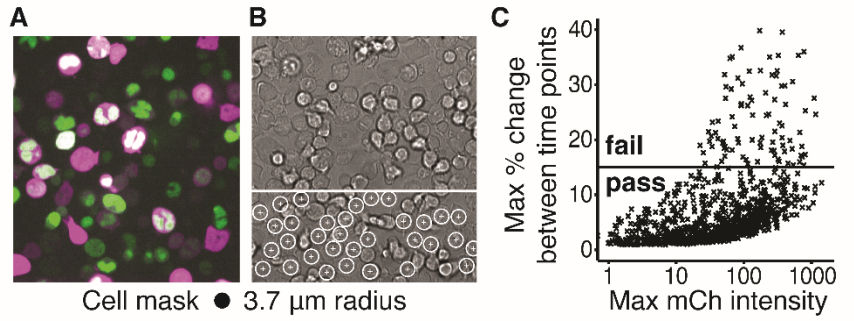

Figure S2: Extraction and QC of single-cell trajectories from time-lapse images. (A) Jurkat Tat-Dendra + LTR mCherry-deg cells underwent time-lapse microscopy to yield the data described in Fig. 3. Briefly, the cells were biotinylated, attached to a streptavidin-coated coverslip, then induced with 250 ng/mL Dox and imaged for 20 hours. Full details of this procedure are in Methods. This two-color fluorescence image is from the final time point of Clone #2, and shows one tile of a 5x5 grid. Tat-Dendra is green; mCherry is magenta. (B) The same location as (A), in brightfield. Cell locations were marked in brightfield to ensure that dim and non-fluorescent cells are fairly represented. The lower section of the image shows the marked cell centers (white +) surrounded by a 23-pixel diameter circle, which is taken as the cell's area. Pixels within this area contribute to the fluorescence intensity of the cell. This location is used for all time points to create a single-cell trajectory. (C) To reduce noise in the data, trajectories that showed excessive changes between consecutive time points were discarded. This image shows raw mCherry trajectories from Clone #2 undergoing QC. The maximum percent change between two consecutive time points is plotted as a function of maximum intensity, showing that for both dim and bright cells, most have a percent change under 10%. To pass QC, both Dendra and mCherry channels must be under the 15% noise cutoff shown. These raw trajectories underwent further QC, smoothing, and bleaching correction, as detailed in Methods and Fig. S3.

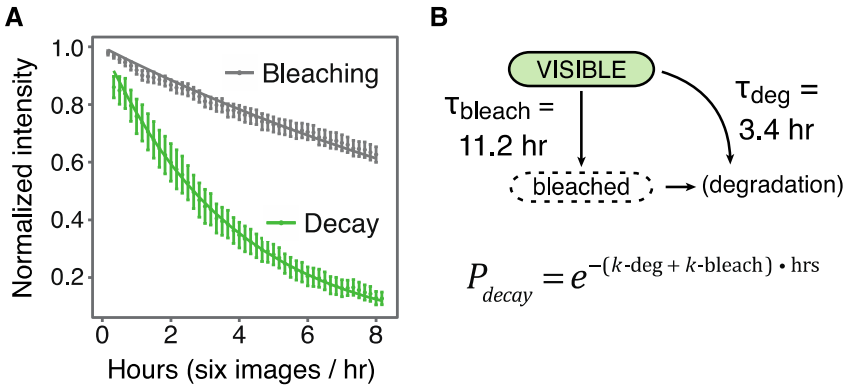

Figure S3: Correcting for photobleaching in Tat-Dendra trajectories. (A) Single-cell trajectories were constructed from time-lapse imaging of bright Jurkat Tat-Dendra cells. For the decay curve, cycloheximide was added at t=0 to stop protein synthesis, and images were taken every 10 minutes. For the bleaching curve, the same number of images was taken in 5-second intervals to simulate non-decaying protein. Error bars show 95% CI. (B) These trajectories were fit to simple exponential decay models. The bleaching half-time was measured at 11.2 hours. The total rate of visible protein decay can be expressed as the sum of the bleaching and degradation rates; from this equation, the half-life of Tat-Dendra was calculated at 3.4 hours. This value was confirmed by flow cytometry experiments (data not shown). To compute the amount of non-fluorescent protein present, we assume that a fraction of Tat-Dendra enters the bleached state at each time point, and the bleached protein degrades at the normal rate.

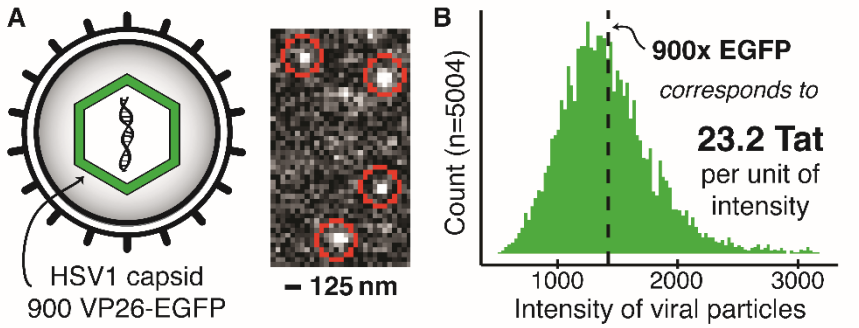

Figure S4: Quantitation of Tat-Dendra by HSV-GFP molecular standard. (A) HSV-GFP viral particles can serve as a "molecular ruler" to convert fluorescence intensity to molecular number. Since the HSV capsid protein VP26 is fused to EGFP, and each viral particle assembles into an icosahedron with precisely 900 copies of VP26, each viral particle contains 900 EGFP molecules. A small portion of a representative image of HSV-GFP is shown; diffraction-limited viral particles that were successfully segmented are circled in red. (B) Histogram of intensities from all viral particles (n=5004) that were identified, showing a roughly normal distribution with a mean of 1424 intensity units per particle. An increase of one intensity unit corresponds to 23.2 Tat-Dendra molecules; this conversion is detailed in Methods.

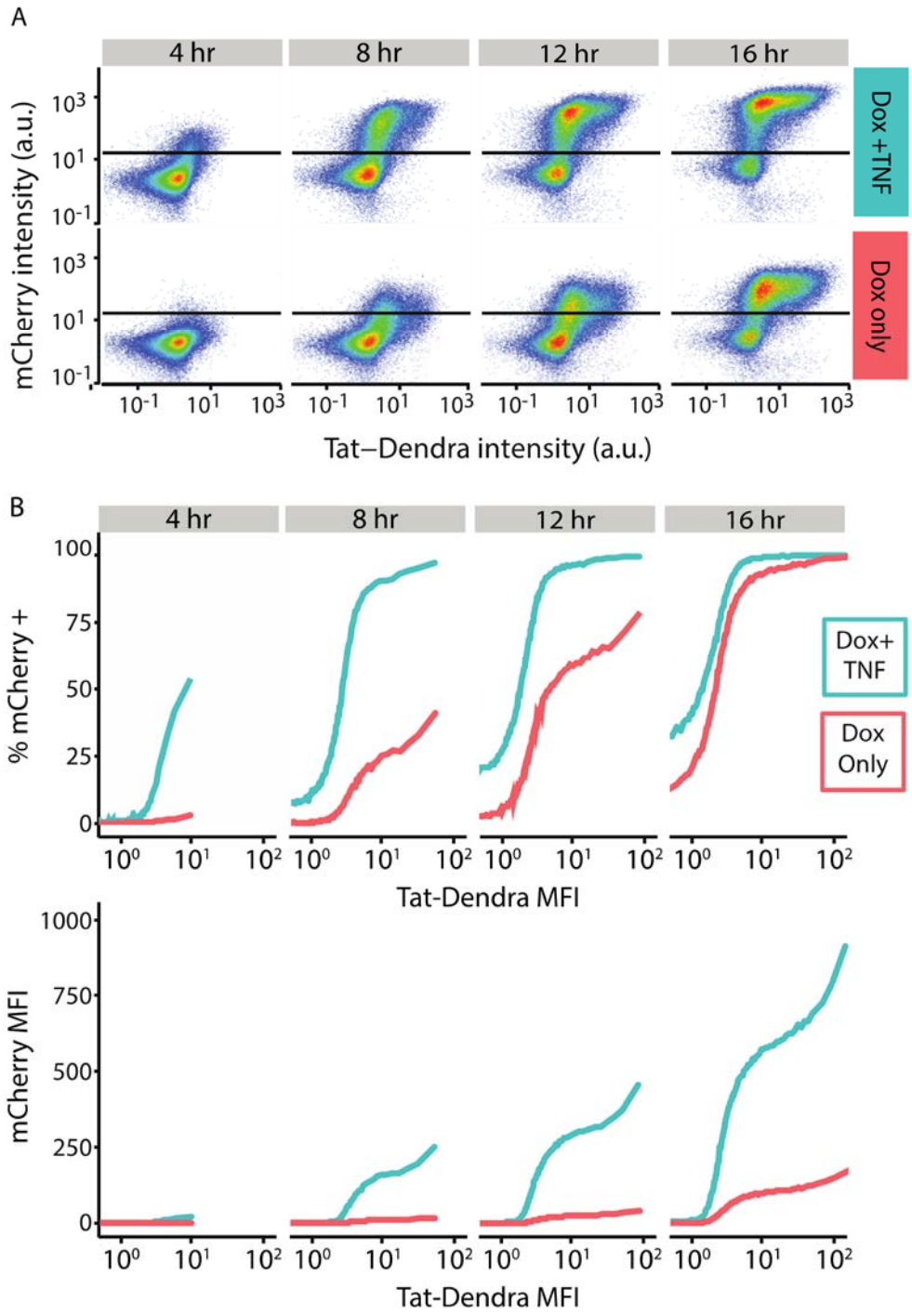

Figure S5: LTR activation by TNF shortens the lifetime of transient Tat-activation threshold. (A) Flow cytometry time-course (as in Fig 2) for Jurkat LTR isoclone #4. Horizontal line indicates the mCherry positive cutoff; 10,000 randomly sampled cells displayed. (B) Dose-response curves for % mCherry positive cells (top) and mCherry MFI (bottom) from data in panel A. Individual cells were ranked by Dendra intensity and sorted into 100 bins based on percentile. Each bin contained a minimum of 3,000 cells. Percentage of cells above the mCherry positive cutoff and median mCherry and Dendra fluorescence were calculated for each bin.

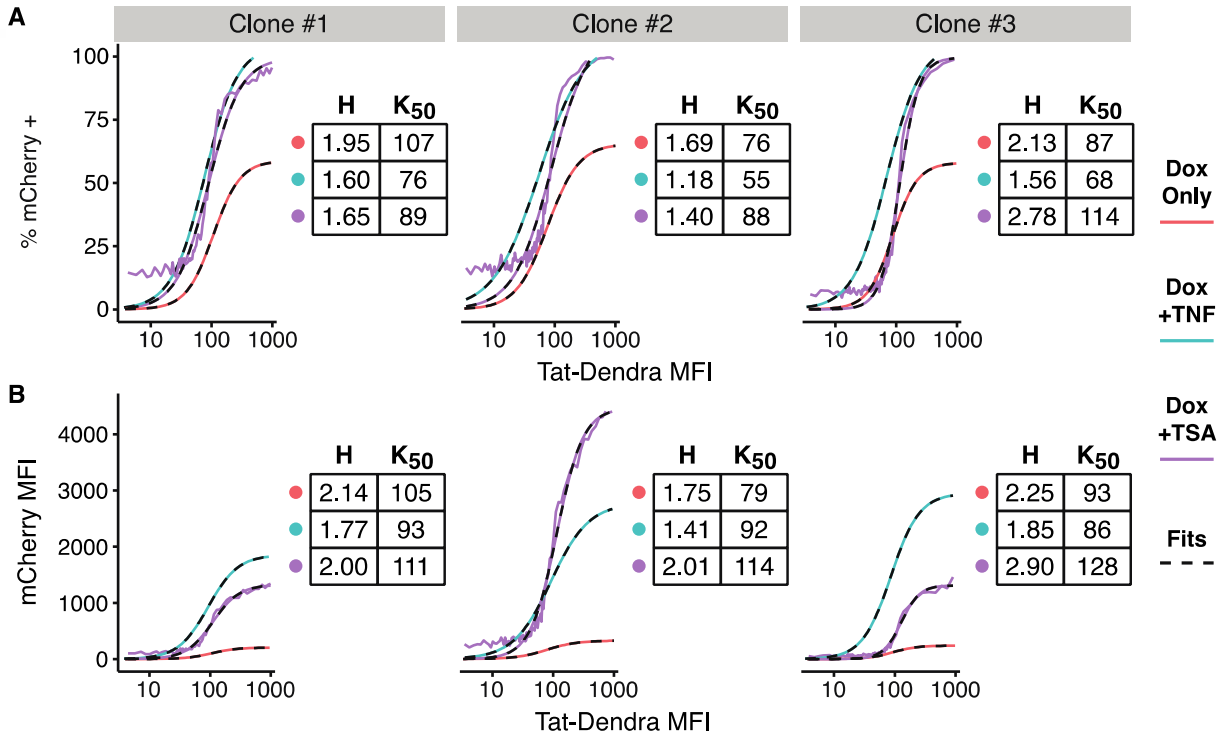

Figure S6: The non-physiological activator TSA and the cytokine TNF have distinct effects on threshold parameters. (A) Dose-response curves for %mCherry positive cells from flow cytometry measurements of three isoclones of Jurkat Tet-Tat-Dendra + LTR-mCherry, at 20 hours post Dox induction in the presence of TSA (trichostatin A, a histone deacetylase inhibitor). Each data point depicts a group of 500 cells. These data were fit to a Hill function (dashed lines), with Hill coefficient (*H*) and half-maximal binding (K_{50}) values in adjacent table. Hill fits from Fig. 4 are presented for comparison. (B) Dose-response curves from the above experiment, showing mCherry MFI. While TNF consistently decreases *H* and K_{50}, TSA has a less consistent effect on both parameters.

Mathematical Modeling Appendix

Based on previous literature (Ha and Ferrell, 2014), we explored a number of different models in an attempt to recapitulate the threshold response observed in the data. We began by examining previous models (Weinberger and Shenk, 2007) with acetylation de-acetylation cycles in Tat feedback, since such enzymatic 'futile cycles' can lead to ultrasensitive responses udner certain conditions (Ha and Ferrell, 2014). We exmaine these models in both the steady-state and pre-steady-state regime. For simplicity, we examine highly course-grained models where transcription and translation processes are represented by lumped parameters.

■ Reversible Acetylation of Tat (analysis of model from Weinberger & Shenk, *PLoS Biol.* 2007)

In this model, Tat is expressed in an deacetylated form (Tat_d) and can be acetylated at lysinses (the K50 or K51 residues) to produce acetylated Tat (Tat_A) that is required for transactivation of the LTR promoter to ultimately produce mCherry (transcription and translation are represented by lumped parameters).

$$\left(\begin{array}{c} \frac{d\,\text{Tat}_d(t)}{\text{dt}} = \beta - k_A\,\text{Tat}_d(t) + k_d\,\text{Tat}_A(t) - \delta_{\text{tat}}\,\text{Tat}_d(t) \\ \frac{d\,\text{Tat}_A(t)}{\text{dt}} = k_A\,\text{Tat}_d(t) - k_d\,\text{Tat}_A(t) \\ \frac{d\,\text{mCherry}(t)}{\text{dt}} = \alpha\,\text{Tat}_A(t) - \delta_{\text{mch}}\,\text{mCherry}(t) \end{array}\right)$$

Where β is the lumped rate of dox-induced Tat production, k_A and k_d, are the rates of Tat acetylation and deacetylation, respectively, α is the lumped rate of mCherry production, based on acetylated Tat transctivation of the LTR, and δ_{tat} and δ_{mch} are the per capita protein decay rates for mCherry and Tat, respecitvely. The steady states can easily be solved:

$$\left(\overline{\text{Tat}_A} \to \frac{\beta\,k_A}{k_d\,\delta_{\text{tat}}} \quad \overline{\text{Tat}_d} \to \frac{\beta}{\delta_{\text{tat}}} \quad \overline{\text{mCherry}} \to \frac{\alpha\,\text{Tat}_A}{\delta_{\text{mch}}}\right)$$

and a straightforward algebraic rearrangement shows that mCherry's steady state scales as a linear function of the Tat_d steady state. This can also be seen by plotting mCherry as a function of Tat using a parametric plot in *Mathematica*™ (using the parameters $\{\alpha \to 10,\ k_A \to 0.01,\ k_d \to 1,\ \delta_{\text{tat}} \to 0.25,\ \delta_{\text{mch}} \to 0.2\}$ and allowing β to vary between [0,20])

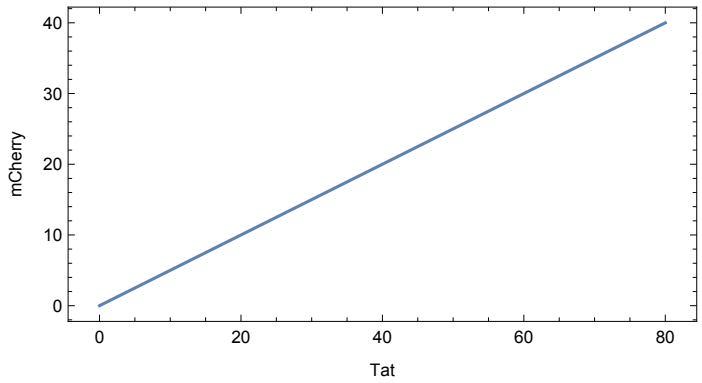

This simple model can be analytically solved in the pre-steady-state regime (and plotted using the parameter estimates above):

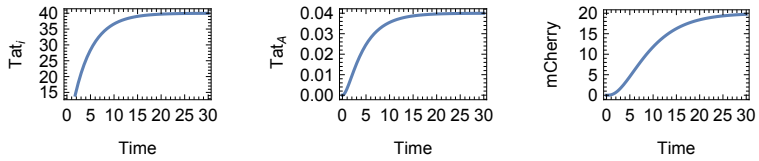

This analytical solution allows analysis of mCherry vs. Tat in the pre-steady-state regime using the parametric plotting function in *Mathematica* (β varying from [0,10] in this case):

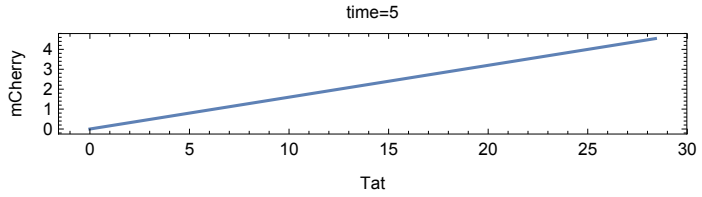

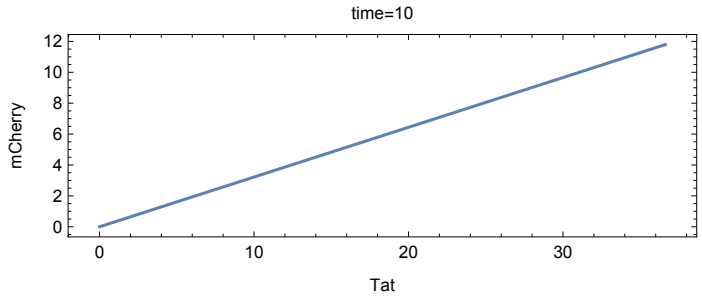

Clearly, this model does not generate a threshold response in either the steady-state or pre-steady-sate regime.

▫ *Saturable version of 2007 model*

Since the above model uses mass-action kinetics for acetylation and well-known examples of ultrasensitivty depend on conversion reactions being in the saturated (non mass action) zero-order regime (Ha and Ferrell, 2014), we also explored a saturable version of this model:

$$\frac{d\,\mathrm{Tat}_d(t)}{dt} = \frac{k_d\,\mathrm{Tat}_A(t)}{\mathrm{Tat}_A(t)+k_M} - \frac{k_A\,\mathrm{Tat}_d(t)}{\mathrm{Tat}_d(t)+k_M} + \beta - \delta_{\mathrm{tat}}\,\mathrm{Tat}_d(t)$$

$$\frac{d\,\mathrm{Tat}_A(t)}{dt} = \frac{k_A\,\mathrm{Tat}_d(t)}{\mathrm{Tat}_d(t)+k_M} - \frac{k_d\,\mathrm{Tat}_A(t)}{\mathrm{Tat}_A(t)+k_M}$$

$$\frac{d\,\mathrm{mCherry}(t)}{dt} = \frac{\alpha\,\mathrm{Tat}_A(t)}{\mathrm{Tat}_A(t)+k_M} - \delta_{\mathrm{mch}}\,\mathrm{mCherry}(t)$$

which yields steady states:

$$\left(\begin{array}{c} \mathrm{Tat}_A \to -\frac{\beta\,k_A}{\beta\,k_A-\beta\,k_d-k_d\,\delta_{\mathrm{tat}}} \\ \mathrm{Tat}_d \to \frac{\beta}{\delta_{\mathrm{tat}}} \\ \mathrm{mCherry} \to -\frac{\alpha\,\beta\,k_A}{\delta_{\mathrm{mch}}\,(\beta\,k_A-\beta\,k_d-k_d\,\delta_{\mathrm{tat}})} \end{array}\right)$$

but which still generates a hyperbolic response in steady state as visualized by a parametric plot (with $k_M = 1,\ \alpha = 100,\ \beta$ varied from $[0,\ 20]$ and other parameters as above):

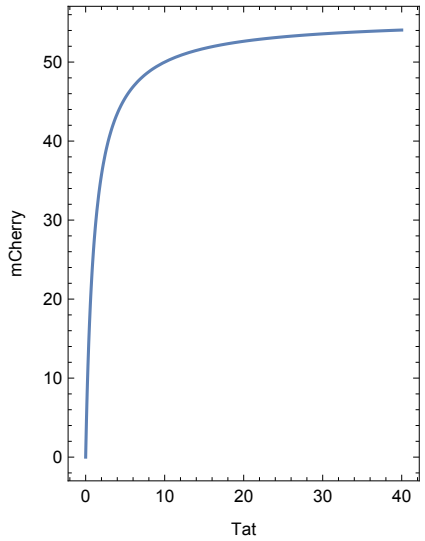

Numerical solutions of this model also generate a hyperbolic dose-response functions in the pre-steady-state regime as plotted using a numerical parametric plotting function (β varied from [0,20] all other parameters as above):

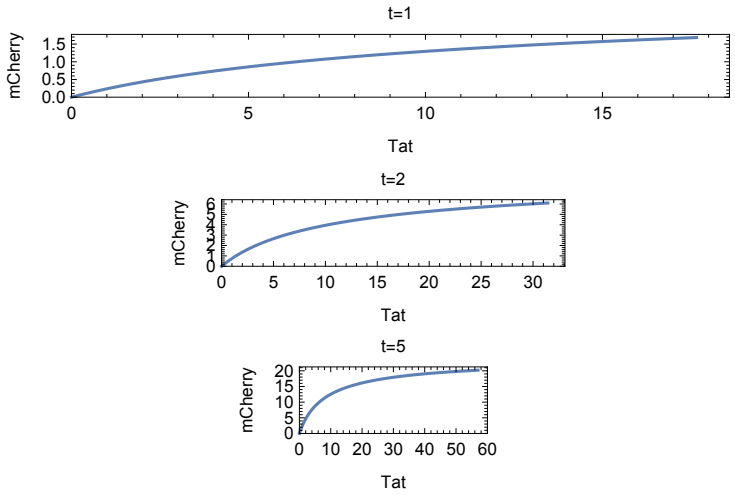

■ Multi-site Reversible Acetylation of Tat

We also explored an extended model with additional acetylation steps:

$$\frac{d\,\mathrm{Tat}_d(t)}{dt} = k_d\,\mathrm{Tat}_A(t) - k_A\,\mathrm{Tat}_d(t) + \beta - \delta_{\mathrm{tat}}\,\mathrm{Tat}_d(t)$$

$$\frac{d\,\mathrm{Tat}_A(t)}{dt} = -k_d\,\mathrm{Tat}_A(t) + k_A\,\mathrm{Tat}_d(t) - k_A\,\mathrm{Tat}_A(t) + k_d\,\mathrm{Tat}_{\mathrm{A2}}(t)$$

$$\frac{d\,\mathrm{Tat}_{\mathrm{A2}}(t)}{dt} = k_A\,\mathrm{Tat}_A(t) - k_d\,\mathrm{Tat}_{\mathrm{A2}}(t)$$

$$\frac{d\,\mathrm{mCherry}(t)}{dt} = \alpha\,\mathrm{Tat}_{\mathrm{A2}}(t) - d_{\mathrm{mch}}\,\mathrm{mCherry}(t)$$

which yields the following steady states:

$$\left(\begin{array}{c} \mathtt{Tat_A} \to \frac{\beta\,\mathtt{k_A}}{\mathtt{k_d}\,\delta_{\mathtt{tat}}} \\ \mathtt{Tat_d} \to \frac{\beta}{\delta_{\mathtt{tat}}} \\ \mathtt{Tat_{A2}} \to \frac{\beta\,\mathtt{k_A^2}}{\mathtt{k_d^2}\,\delta_{\mathtt{tat}}} \\ \mathtt{mCherry} \to \frac{\alpha\,\beta\,\mathtt{k_A^2}}{\mathtt{k_d^2}\,\delta_{\mathtt{mch}}\,\delta_{\mathtt{tat}}} \end{array}\right)$$

which, as above, show that the dose-response of mCherry is linear with respect to Tat_d and shows implicitly that increasing the number of acetylation sites will not change the linear response to Tat (since the nonlinearity appears only in the rate constants k_A and k_d not in other parameters). For completeness, we show that plots of the steady-states response of this model yielded a hyperbolic dose-response function at steady state as visualized by a parametric plot:

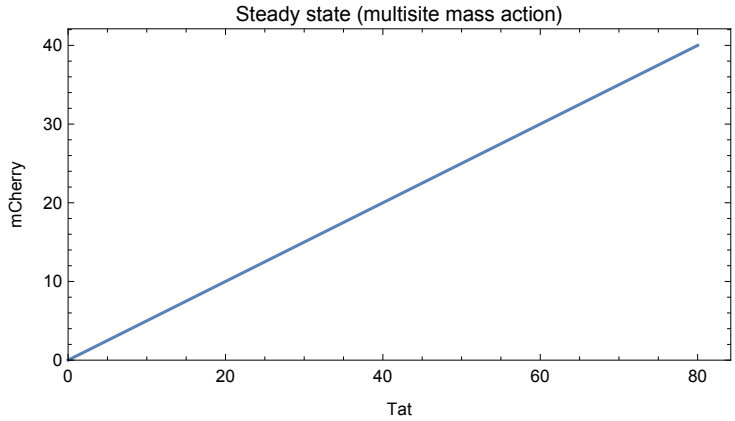

We also examined the pre-steady-state regime for this multi-site acetylation model and found that it also yields hyperbolic dose-response function (all parameters as above)

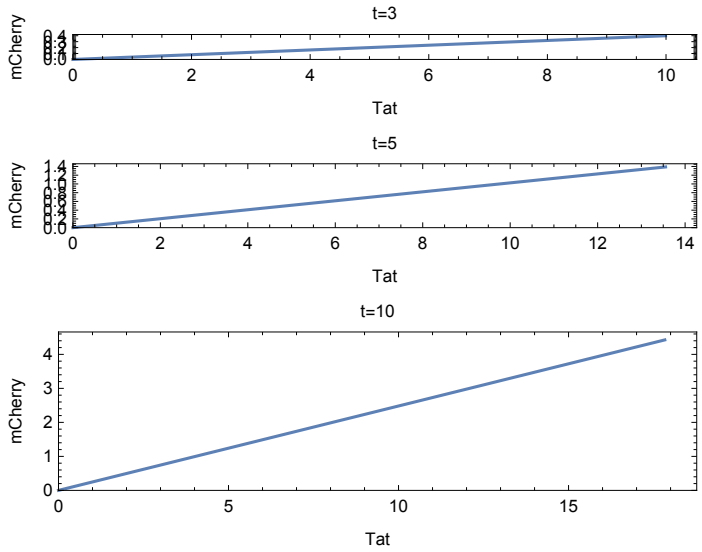

▫ *Saturable version of Multi-site Reversible Acetylation of Tat*

The saturable version of this model:

$$\frac{d\,\mathrm{Tat}_d(t)}{dt} = -\frac{k_A\,\mathrm{Tat}_d(t)}{\mathrm{Tat}_{id}(t)+1} + \frac{k_d\,\mathrm{Tat}_A(t)}{\mathrm{Tat}_A(t)+1} + \beta - \delta_{\mathrm{tat}}\,\mathrm{Tat}_i(t)$$

$$\frac{d\,\mathrm{Tat}_A(t)}{dt} = -\frac{k_d\,\mathrm{Tat}_A(t)}{\mathrm{Tat}_A(t)+1} + \frac{k_A\,\mathrm{Tat}_d(t)}{\mathrm{Tat}_d(t)+1} - \frac{k_A\,\mathrm{Tat}_A(t)}{\mathrm{Tat}_A(t)+1} + \frac{k_d\,\mathrm{Tat}_{A2}(t)}{\mathrm{Tat}_{A2}(t)+1}$$

$$\frac{d\,\mathrm{Tat}_{A2}(t)}{dt} = \frac{k_A\,\mathrm{Tat}_A(t)}{\mathrm{Tat}_A(t)+1} - \frac{k_b\,\mathrm{Tat}_{A2}(t)}{\mathrm{Tat}_{A2}(t)+1}$$

$$\frac{d\,\mathrm{mCherry}(t)}{dt} = \frac{\alpha\,\mathrm{Tat}_{A2}(t)}{\mathrm{Tat}_{A2}(t)+1} - \delta_{\mathrm{mch}}\,\mathrm{mCherry}(t)$$

Yields steady states:

$$\left(\begin{array}{c} \mathrm{Tat}_A \to -\frac{k_A\,\mathrm{Tat}_d\,k_M}{k_A\,\mathrm{Tat}_d - k_b\,\mathrm{Tat}_d - k_b\,k_M} \\ \mathrm{Tat}_i \to \frac{\beta}{\delta_{\mathrm{tat}}} \\ \mathrm{Tat}_{A2} \to -\frac{k_A^2\,\mathrm{Tat}_d\,k_M}{k_A^2\,\mathrm{Tat}_d - k_b^2\,\mathrm{Tat}_d - k_b^2\,k_M} \\ \mathrm{mCherry} \to -\frac{\alpha\,k_A^2\,\mathrm{Tat}_d\,k_M}{\delta_{\mathrm{mch}}\left(k_A^2\,\mathrm{Tat}_d - k_b^2\,\mathrm{Tat}_d - k_b^2\,k_M\right)} \end{array}\right)$$

which produced a qualitatively similar hyperbolic response in the steady-state regime that can be visualized by a parametric plot (α=100, β varied from [0,20], and other parameters as above):

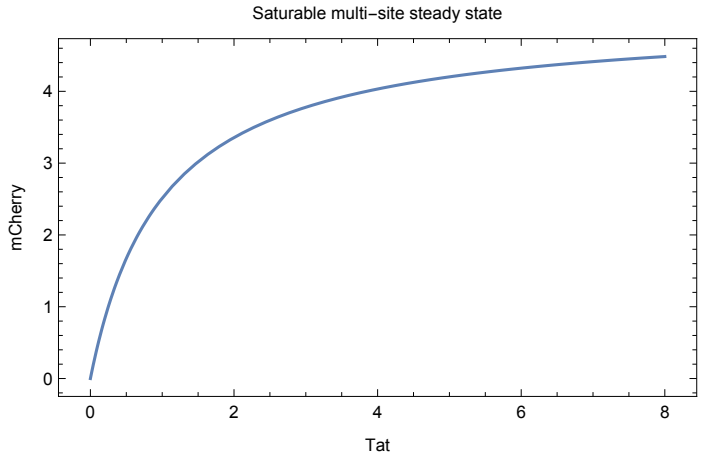

and the pre-steady-state regime (parameters as above):

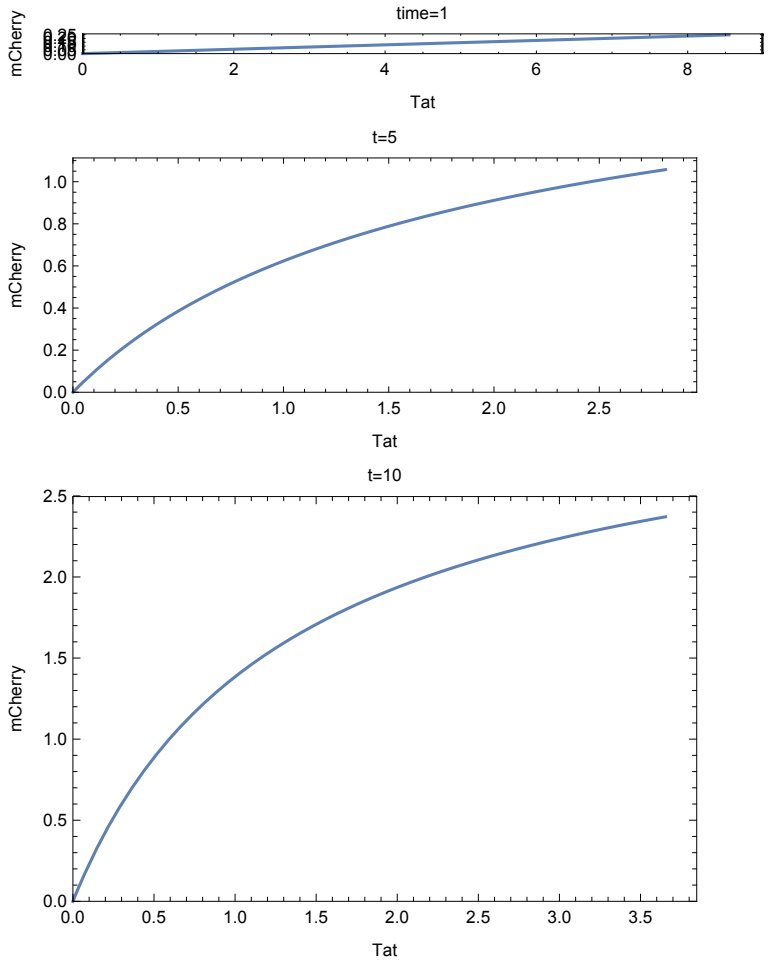

Overall, these results show that in the deterministic regime, models incoporating reversible covalent modifications of Tat (with either mass action or saturable kinetics) could not recapitulate the threshold response.